environmental microbiology

Environmental Microbiology (2022) **24**(3), 1499–1517 doi:10.1111/1462-2920.15925

Cellular adaptation of *Clostridioides difficile* to high salinity encompasses a compatible solute-responsive change in cell morphology

Annika-Marisa Michel,[1,2] José Manuel Borrero-de Acuña,[1,2,3*] Gabriella Molinari,[4] Can Murat Ünal,[1] Sabine Will,[5] Elisabeth Derksen,[1] Stefan Barthels,[1,2] Wiebke Bartram,[1,2] Michel Schrader,[1] Manfred Rohde,[4] Hao Zhang,[1,6] Tamara Hoffmann,[7,8] Meina Neumann-Schaal,[2,5] Erhard Bremer[7,8] and Dieter Jahn[1,2]

[1]*Institute of Microbiology, Technische Universität Braunschweig, Braunschweig, Germany.*

[2]*Braunschweig Integrated Centre of Systems Biology (BRICS), Technische Universität Braunschweig, Braunschweig, Germany.*

[3]*Departamento de Microbiología, Facultad de Biología, Universidad de Sevilla, Av. de la Reina Mercedes, no. 6, Sevilla, CP 41012, Spain.*

[4]*Central Facility for Microscopy, Helmholtz Centre for Infection Research (HZI), Braunschweig, Germany.*

[5]*Leibniz-Institute DSMZ–German Collection of Microorganisms and Cell Cultures, Braunschweig, Germany.*

[6]*School of Life Science and Technology, Changchun University of Science and Technology, No. 7186 Weixing Road, Changchun, 130022, China.*

[7]*Laboratory for Microbiology, Department of Biology, Philipps-Universität Marburg, Marburg, Germany.*

[8]*Center for Synthetic Microbiology (SYNMIKRO), Philipps-Universität Marburg, Marburg, Germany.*

Summary

Infections by the pathogenic gut bacterium *Clostridioides difficile* cause severe diarrhoeas up to a toxic megacolon and are currently among the major causes of lethal bacterial infections. Successful bacterial propagation in the gut is strongly associated with the adaptation to changing nutrition-caused environmental conditions; e.g. environmental salt stresses. Concentrations of 350 mM NaCl, the prevailing salinity in the colon, led to significantly reduced growth of *C. difficile*. Metabolomics of salt-stressed bacteria revealed a major reduction of the central energy generation pathways, including the Stickland-fermentation reactions. No obvious synthesis of compatible solutes was observed up to 24 h of growth. The ensuing limited tolerance to high salinity and absence of compatible solute synthesis might result from an evolutionary adaptation to the exclusive life of *C. difficile* in the mammalian gut. Addition of the compatible solutes carnitine, glycine-betaine, γ-butyrobetaine, crotonobetaine, homobetaine, proline-betaine and dimethylsulfoniopropionate restored growth (choline and proline failed) under conditions of high salinity. A bioinformatically identified OpuF-type ABC-transporter imported most of the used compatible solutes. A long-term adaptation after 48 h included a shift of the Stickland fermentation-based energy metabolism from the utilization to the accumulation of L-proline and resulted in restored growth. Surprisingly, salt stress resulted in the formation of coccoid *C. difficile* cells instead of the typical rod-shaped cells, a process reverted by the addition of several compatible solutes. Hence, compatible solute import via OpuF is the major immediate adaptation strategy of *C. difficile* to high salinity-incurred cellular stress.

Introduction

Clostridioides difficile (previously *Clostridium difficile*) is a Gram-positive, spore-forming anaerobic pathogen of the gastrointestinal tract, and the leading cause of bacterial healthcare-associated diarrhoea (Hall and O'Toole, 1935; Bartlett *et al*., 1977; Schäffler and Breitrück, 2018). As a formidable human pathogen, it imposes a considerable burden on the health care system in industrial countries due to long hospitalization times of patients and high recurrence rates after initial successful antibiotic treatment (Lessa *et al*., 2015; Shah *et al*., 2016; Hopkins and Wilson, 2018; Zhang *et al*., 2018). The symptoms of *C. difficile* incurred disease range from mild self-resolving diarrhoea to deadly toxic colon (Abt *et al*., 2016).

Received 27 November, 2021; revised 24 January, 2022; accepted 25 January, 2022. *For correspondence. E-mail jbdeacuna@us.es; Tel. +34-954557116; Fax +34-954557830.

The clinically most relevant form of *C. difficile* infections is pseudomembranous colitis, a severe inflammation of colon tissue accompanied by perturbation of the epithelial barrier and infiltration by immune cells (Abt *et al*., 2016; Guery *et al*., 2019). Many of the pathological consequences of the infection process are connected to the activities of two toxins (TcdA and TcdB) produced by *C. difficile* (Rupnik *et al*., 2009). Efficient colonization of the human colon by *C. difficile* require several traits, most of which are not well understood (Guarner and Malagelada, 2003; Britton and Young, 2014; Abt *et al*., 2016). One of the conditions encountered by *C. difficile* during the infection process in all likelihood are ionic challenges as concentration of NaCl up to 350 mM can be reached in the intestine (Fordtran and Locklear, 1966; Sleator *et al*., 2007; Overduin *et al*., 2014).

Most bacteria have evolved highly integrated adaptive responses to high osmolarity- and high ionic strength-incurred cellular stress. These aim in their core to counteract loss of water from the cell and thereby prevent the ensuing increase in molecular crowding of the cytoplasm and growth-impairing drop in turgor (Wood, 2011; van den Berg *et al*., 2017; Bremer and Krämer, 2019). Those bacteria that follow the *salt-out* adjustment response (Galinski and Trüper, 1994; Kempf and Bremer, 1998; Gunde-Cimerman *et al*., 2018) initially increase their cytoplasmic potassium pool upon exposure to high salinity/osmolarity surroundings to raise the osmotic potential of the cytoplasm thereby curbing water efflux (Wood, 2011; Bremer and Krämer, 2019). However, the development of a long-lasting high-ionic strength cytoplasm is avoided by the microbial *salt-out* responders as they subsequently replace, at least partially, the prior imported K^+-ions by physiologically and biochemically highly compliant organic osmolytes, the so-called compatible solutes (Kempf and Bremer, 1998; Gunde-Cimerman *et al*., 2018).

The amassing of compatible solutes by osmotically stressed microbial cells can typically be achieved both via their synthesis and import and provides the cells with a considerable flexibility to ensure growth and survival under both suddenly imposed and sustained adverse ionic or osmotic conditions (Wood, 2011; Bremer and Krämer, 2019). It is thus not surprising that major human pathogens (e.g. *Listeria monocytogenes*, *Salmonella typhimurium*, *Vibrio cholerae*, *Staphylococcus aureus*) use the *salt-out* response in order to successfully colonize their eukaryotic hosts (Sleator and Hill, 2001; Wood *et al*., 2001; Casey and Sleator, 2021; Gregory and Boyd, 2021).

Despite the apparent relevance of ionic stress for the physiology *of C. difficile* in its primary ecological niche (Fordtran and Locklear, 1966; Sleator *et al*., 2007; Overduin *et al*., 2014), no in-depth study on how this human pathogen copes with high salinity incurred ionic challenges has so-far been reported. Here, we have studied the physiological and molecular adaptation of *C. difficile* to conditions of sustained high salinity. By assessing the metabolomic profile of salt-stressed and non-stressed cells, we observed that *C. difficile*, in notable contrast to many other bacteria (Kempf and Bremer, 1998; Gunde-Cimerman *et al*., 2018), apparently does not synthesize compatible solutes in a short-term response when challenged by high salinity on a sustained basis, a finding that correlates well with its rather salt-sensitive growth profile. However, *C. difficile* can counteract the detrimental effects of high salinity on growth through the import of various compatible solutes, an adaptive process that relies on the activity of an OpuF-type ABC transport system (Teichmann *et al*., 2018). Long-term adaption to high saline surroundings was achieved via a re-programming of the central energy metabolism resulting in the accumulation of the energy substrate and compatible solute L-proline, a process that contributed to growth under unfavourable high salinity conditions. Strikingly, *C. difficile* also responds to sustained high salinity through a transition from its typical rod-shaped cell morphology to a coccoid cell form, a process that can be reversed through the import of compatible solutes.

Results

The addition of 400 mM NaCl severely restricts growth of C. difficile *630Δ*erm

To study the salt stress response of *C. difficile*, we employed the *C. difficile* model strain 630Δ*erm* (Dannheim *et al*., 2017). We used for growth experiments a chemically defined minimal medium (MDM) (Table S1). We increased the osmolarity and ionic strength of this basal medium by adding different amounts of NaCl to it (final concentrations: 100, 200, 300, 350, 400 mM), conditions that linearly increased the osmolarity of the basal growth medium from 244 mOsmol kg^{-1} of MDM to 1023 mOsmol kg^{-1} when 400 mM NaCl was added (Fig. S1). This experimental set-up increased not only the osmolarity of the growth medium but also affected its ionic strength (Wood, 2011; Bremer and Krämer, 2019). We note in this context that concentration of up to 350 mM NaCl can be reached in the intestine (Fordtran and Locklear, 1966; Sleator *et al*., 2007; Overduin *et al*., 2014).

Cells of *C. difficile* strain 630Δ*erm* were able to grow in the presence of 100 and 200 mM of additional NaCl without strong effects in doubling time or lag phase in comparison to their growth in the basal MMD-medium

Table 1. Bacterial strains used in this study.

Strain	Features	Reference
E. coli		
DH10B	Strain for cloning and plasmid propagation, F$^-$ *mcrA* Δ*(mrr-hsdRMS-mcrBC) φ80lacZΔM15 ΔlacZX74 recA1 endA1 araD139* Δ*(ara-leu)7697 galU galK λ-rpsL(*Str^R*) nupG*	Thermo Fisher scientific, Waltham, USA
CA434	*E. coli* HB101 carrying the Incβ conjugative plasmid R702 (F-, *thi*-1,hsdS20(r_B-m_B-), *sup*E44, *recA*13, ara-14, *rps*L20(Str^R), *leu*B6,*gal*K2,*xyl*-5,*mtl*-1)	Purdy *et al*. (2002)
B. subtilis		
JH642	wild type; *trpC2*, *pheA1*	Brehm *et al*. (1973)
TMB118	JH642 Δ(*opuA*::*tet*)3 Δ(*opuC*::*spc*)3 Δ*opuD*::*kan*)2 Δ*opuB*::*erm*)1	Teichmann *et al*. (2017)
AM01	TMB118 *amyE*:: *opuF*$_{C.\ difficile\ 630\Delta erm}$ (*CDIF630erm_01020*:: *CDIF630erm_01021*)	This work
AM02	TMB118 *amyE*::uTS $_{C.\ difficile630\Delta erm}$ (*CDIF630erm_03510*:: *CDIFerm630_03509*)	This work
C. difficile		
630Δ*erm* (DSM28645)	wild type, erythromycin sensitive mutant of *C. difficile* 630, Thi^R	Hussain *et al*. (2005)
Δ*opuFB*	*opuFB* (*CDIF630erm_01021*; annotated as *opuCC*) insertional mutant of *C. difficile* 630Δ*erm*, target site 936l937 sense (936l937s::intron *ermB*), Thi^R, Erm^R	This work

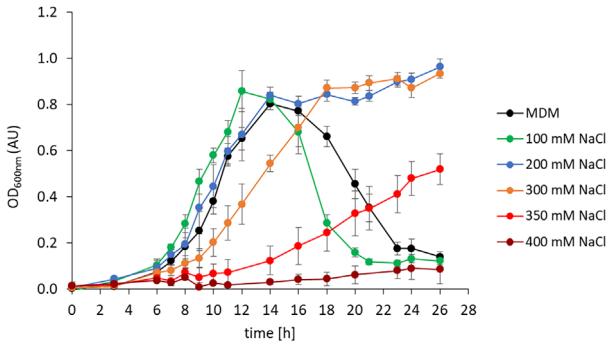

Fig. 1. Salt tolerance of *C. difficile* 630Δ*erm*. *Clostridioides difficile* 630Δ*erm* was grown in MDM medium either without additional NaCl (black line) or with additional 100 mM (green line), 200 mM (blue line), 300 mM (orange line), 350 mM (red line) or 400 mM NaCl (brown line). Growth was monitored via OD_{600nm} measurements over 26 h. Growth experiments were performed with at least four biological and three technical replicates. The standard deviation is given.

(Fig. 1). The presence of 200 mM NaCl in the growth medium led to a stationary plateau in biomass formation after 14 h of growth, whereas the optical densities of the cultures growing without NaCl, or with only 100 mM NaCl, strongly dropped after reaching their maximal cell density (Fig. 1). The physiological reasons for the growth patterns of these two latter cultures are currently unknown. Further increases in the salt concentration (300 and 350 mM) stepwise impaired growth of *C. difficile* strain 630Δ*erm*, until it was almost completely abolished in the presence of 400 mM for the first 18 h of incubation. This effect was overcome by long-term incubation of the culture (for 48 h), where growth resumed after 35 h. The molecular basis of this late adaptation was investigated by metabolomics and is described below. Overall, these observations allowed for the distinction of two time-resolved phases of high salt adaption of *C. difficile*: the immediate response in the first 12 h which is limited to concentrations of up to 300 mM NaCl and a long-term adaption after 35–40 h to 350 mM salt and higher. In the following parts, we mainly focused on the short-term adaptation to increased salt concentrations. Overall, one can conclude from this set of growth experiments that *C. difficile* strain 630Δ*erm* seems to be a rather salt-sensitive bacterium (Fig. 1).

Many bacteria synthesize various types of compatible solutes when they are exposed to high salinity or high osmolarity surroundings to counteract the detrimental effects of such conditions on cellular hydration, magnitude of turgor and growth (Kempf and Bremer, 1998). Glycine betaine, ectoine and trehalose are widely used members of the compatible solutes. We, therefore, searched the genome sequence of *C. difficile* strain 630Δ*erm* (Dannheim *et al*., 2017) for the presence of the corresponding biosynthetic genes. In agreement with the rather salt-sensitive growth profile of this strain (Fig. 1), no genes for the biosynthesis of glycine betaine, ectoine or trehalose were detected.

Bioinformatic-based identification of potential compatible solute transporters in C. difficile

Most bacteria possess import systems for the acquisition of compatible solutes, osmotic stress-relieving organic osmolytes (Wood, 2011; Bremer and Krämer, 2019). In the genome sequence of *C. difficile* strain 630Δ*erm* [genome accession number CP016318] (Dannheim *et al*., 2017), genes for two putative ABC-type compatible solute transporters are annotated; *CDIF630erm_01020/01021* (*CD630_09000/09010*) and *CDIF630erm_03509/03510* (*CD630_32150/32160*) respectively. Analysis of the genetic setup of their coding regions showed a similar molecular arrangement for both putative binding-protein dependent transport systems (Fig. 2A). Both operons consist of two genes. One encodes a cytoplasmic ATPase (CDIF630erm_01020 and CDIF630erm_03509 respectively) and the second gene encodes a hybrid protein that comprises an N-terminal transmembrane domain and a C-terminal substrate-binding domain. These two putative compatible solute ABC transporters of *C. difficile* differed thus in their genetic organization from that of the archetypical compatible solute transporters OpuA, OpuB and OpuC of the Gram-positive bacterium *Bacillus subtilis* which consist of separate genes encoding the transmembrane proteins and the substrate-binding proteins. In these transporters, the substrate-binding proteins are anchored via lipid modification at their N-termini to the outer face of the cytoplasmic membrane (Hoffmann and Bremer, 2017). The putative compatible solute ABC transporters from *C. difficile* resembled in their subunit structure that of the BilE transporter of *L. monocytogenes* (Ruiz *et al*., 2016), the OpuA system from *Lactococcus lactis* (Sikkema *et al*., 2020), and the OpuF transporter from *Bacillus infantis* (Teichmann *et al*., 2018), all of which possess fused transmembrane and substrate-binding proteins (Fig. 2A).

An amino acid sequence alignment of the *C. difficile* strain 630Δ*erm* transporter subunits (CDIF630erm_01021 and CDIF630erm_03510 respectively) with the OpuBC and OpuCC substrate-binding proteins from *B. subtilis* and those of substrate-binding protein domains of the *L. monocytogenes* BilE (Uniprot accession number for BilEB: Q93A34) and of the *B. infantis* OpuF system (Uniprot accession number for OpuFB: U5LFB4) revealed a higher amino acid sequence identity of the substrate-binding domain of the *C. difficile* proteins with that of the OpuF transporter (Fig. 2). The amino acid sequence identity of CDIF630erm_01021 to those of the BilEB, OpuFB and $OpuCC_{Bsub}$ substrate-binding protein domains was 39.0%, 37.8% and 35.3% respectively. Overall CDIF630erm_01021 was somewhat closely related to these reference proteins than CDIF630erm_03510, which displayed amino acid sequence similarities of 36.1%, 35.6% and 32.0% respectively (Fig. 2B). In the light of the sequence homology and the genetic composition, we suggest renaming this previously as OpuC annotated transporter (CDIF630erm_01020/CDIF630erm_01021) (Dannheim *et al*., 2017) to OpuF, a system consisting of the ABC-subunit OpuFA (CDIF630erm_01020) and the fused membrane and substrate-binding protein containing subunit OpuFB (CDIF630erm_01021), as previously defined for the OpuF transporter from *B. infantis* (Teichmann *et al*., 2018).

The substrate-binding domains of compatible solute transporters for ligands with fully methylated nitrogen head-groups (e.g. glycine betaine, choline, carnitine) possess aromatic amino acids at conserved positions whose side-chains form an aromatic cage, a structural determinant that allows compatible solute binding via cation-Π-interactions (Horn *et al*., 2006; Du *et al*., 2011; Pittelkow *et al*., 2011; Teichmann *et al*., 2017; Sikkema *et al*., 2020). In the $OpuCC_{Bsub}$ protein, these amino acids are Tyr residues at positions 91, 137, 217 and 241. The alignment of the amino acid sequences of the putative substrate-binding domains of *C. difficile* showed corresponding aromatic residues (in CDIF630erm_01021 Tyr305, Tyr351, Tyr454 and Phe430 and in CDIF630erm_03510 Tyr302, Tyr347, Tyr450 and Phe426) (Fig. 2B). Furthermore, another key amino acid for substrate binding is Thr94, a residue that has been implicated to mediate the broad substrate specificity of the *B. subtilis* OpuCC ligand-binding protein (Du *et al*., 2011). This residue was also conserved in both substrate-binding protein domains of the two *C. difficile* ABC transporters; Thr308 in CDIF630erm_01021 and Thr305 in CDIF630erm_03510 (Fig. 2B).

Using the available structural data of BilEB (pdb code: 4z7e) (Ruiz *et al*., 2016) and of $OpuCC_{Bsub}$ (pdb code: 3ppn) (Du *et al*., 2011) and by applying the Swiss-Model algorithm (Waterhouse *et al*., 2018), we established an *in silico* model of the structure of the CDIF630erm_01021 substrate-binding protein domain. Inspection of this model revealed that the side chains of four aromatic amino acid in the presumed substrate-binding pocket form indeed an aromatic cage (Fig. 2C and D). Likewise, an *in silico* model was generated for the substrate-binding protein domain of the CDIF630erm_03510 protein using BilEB (pdb code: 4z7e) (Ruiz *et al*., 2016) and $OpuCC_{Bsub}$ (pdb code: 3ppn) as templates (Fig. 2E and F). The *in silico* generated structure revealed the formation of a cage formed by the side-chains of four aromatic amino acids.

The proteins encoded by CDIF630erm_01020/01021 (now OpuF) constitute a compatible solute transporter in C. difficile

In order to verify whether the bioinformatically identified binding-protein dependent ABC systems serve indeed as

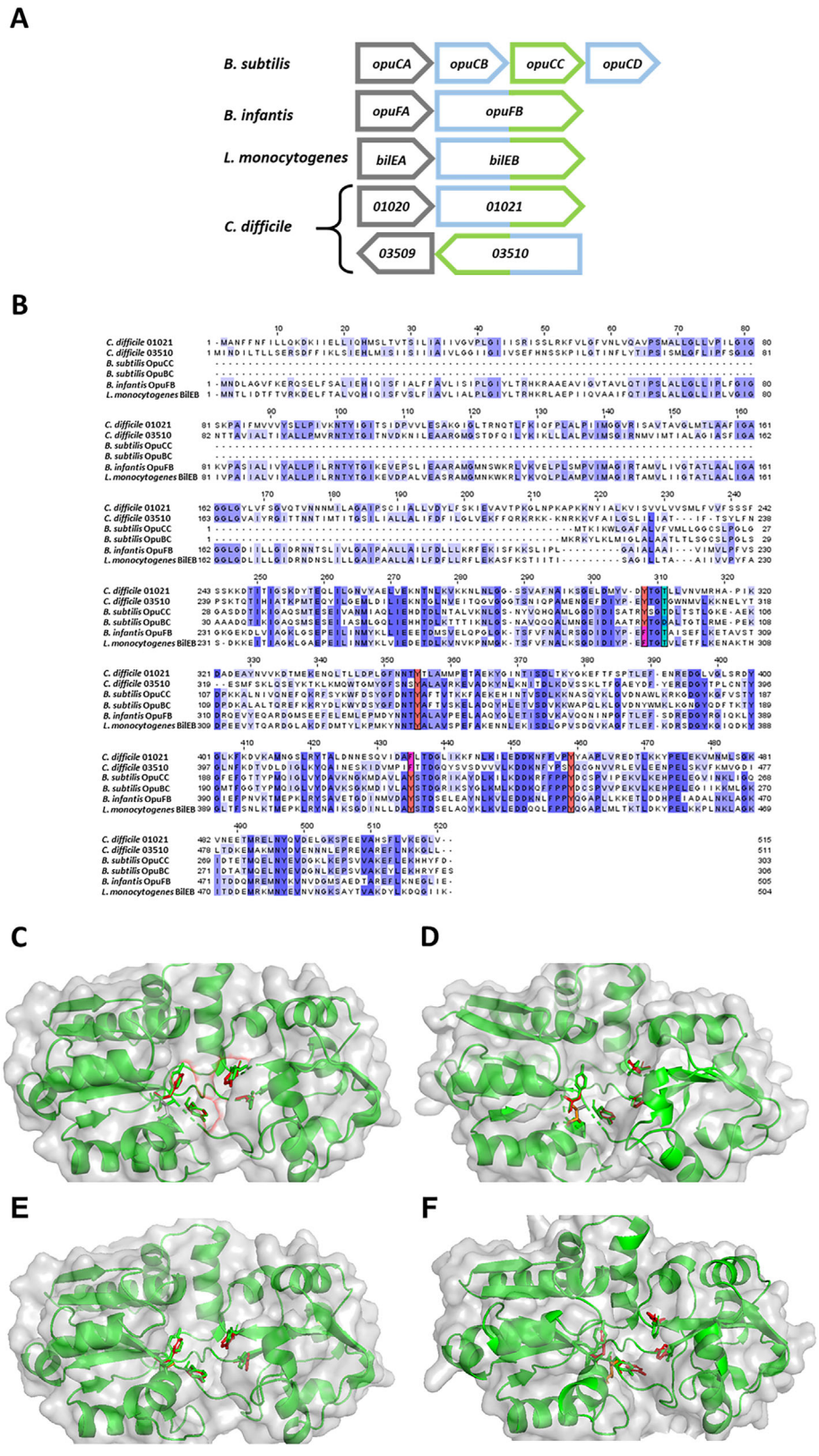

Fig. 2. Comparative structural analyses of putative compatible solute transporters of *C. difficile*.

A. Shown are the genetic organizations of *C. difficile* CDIF630erm_01020/01021 and CDIF630erm_03509/03510 two gene operons in comparison to the four gene operon encoding OpuC-type transporters in *B. subtilis*, the two gene operon for an OpuF-type transporter from *B. infantis*, and two gene operon for a BilE-type of *L. monocytogenes*. CDIF630erm_03509/03510 is located on the complementary strand in reversed gene order. Genes are not drawn to scale, and are coloured according to their function within the protein assembly of the ABC transporter: grey, ATPase-subunit; blue, transmembrane subunit/domain; green, substrate-binding protein/domain.

B. Amino acid sequence alignment of *C. difficile* CDIF630erm_01021 and CDIF630erm_03510 in comparison to substrate-binding proteins of OpuBC and OpuCC from *B. subtilis*, of OpuFB from *B. infantis*, and BilEB of *L. monocytogenes*. Conserved amino acids are highlighted in blue. Conserved amino acid residues constituting the 'hydrophobic cage' implicated in substrate binding are highlighted in red (tyrosines) and in purple (phenylalanines). Threonine 94 in OpuCC, an amino acid determining substrate specificity, is marked green.

C. Comparison of the *in silico* generated structure of the substrate-binding domain of CDIF630erm_01021 with the crystal structure of BilEB (pdb: 4Z7E) or (D) OpuCC (pdb: 3PPN).

E. Comparison of the *in silico* generated structure of the substrate-binding domain of CDIF630erm_03510 with the crystal structure of BilEB (pdb: 4Z7E) or (F) OpuCC (pdb: 3PPN). The computed structures of CDIF630erm_01021 and CDIF630erm_03510 are shown as a green cartoon, whereas the reference structures are shown as white transparent surfaces. The amino acids of the substrate-binding 'hydrophobic cage' are highlighted as green sticks in CDIF630erm_01021 and CDIF630erm_03510, and as red sticks in the reference structures. The key threonine residues in positions 295 and 94 in BilEB and OpuCC respectively, are highlighted as orange sticks.

functional transporters for compatible solutes in *C. difficile*, we carried out complementation assays using the *B. subtilis* strain TMB118 as a well-established screening platform for the activity and substrate profile of compatible solute transporters (Hoffmann and Bremer, 2017). This strain is a derivative of the wild type *B. subtilis* strain JH642, and possesses only the osmostress-adaptive L-proline transporter OpuE, but is devoid of the remaining Opu transporters (OpuA, OpuB, OpuC and OpuD) (Hoffmann and Bremer, 2017; Teichmann *et al*., 2017). Hence, cells of the *B. subtilis* strain TMB118 have lost their capacity to take up and accumulate compatible solutes (except for L-proline) in order to counteract the detrimental effects of ionic- and osmotic-incurred stress on growth. Consequently, strain TMB118 enables the determination of the import activity and substrate spectrum of a putative compatible solute transport system that is recombinantly produced in *B. subtilis*.

We integrated the operons (*CDIF630erm_01020/01021* and *CDIF630erm_03509/03510* respectively) for the putative compatible solute transporters from *C. difficile* as single copies into the non-essential *amyE* locus of strain TMB118, thereby yielding the *B. subtilis* strains AM01 and AM02 respectively. Subsequently, we carried out osmotic stress protection assays in a minimal medium with a panel of compatible solutes known to confer relief from high salinity incurred stress in *B. subtilis* (Hoffmann and Bremer, 2017). For this purpose, the scattered light intensities (SLIs) in dependence of the biomass at 12 h were determined using 48-well FlowerPlates in a BioLector® mini bioreactor system in which the recombinant *B. subtilis* strains AM01 and AM02 were grown in a minimal medium (Fig. S3). Under these conditions, growth of the *B. subtilis* wild type strain JH642 possessing the full set of Opu transporters (Hoffmann and Bremer, 2017) was strongly impaired when the medium contained 1 M additional NaCl, but growth was rescued when 1 mM of 10 different compatible solutes was separately added to the cultures (Fig. 3). In contrast, all tested compatible solutes, except for L-proline, were unable to rescue the growth of the tester strain TMB118 (Fig. 3). Osmostress protection of strain TMB118 by L-proline was expected from previous results and predicted from the genetic set-up of this *B. subtilis* strain (Hoffmann and Bremer, 2017; Teichmann *et al*., 2017).

While the growth of the *B. subtilis* tester strain TMB118 possessing the *C. difficile* genes CDIF630erm_03509/03510 (strain AM02) was not rescued at high salinity by any of the assessed compatible solute (except for L-proline) (Fig. 3), a number of compatible solutes served as osmostress protectants for the recombinant strain AM01 possessing the *C. difficile* CDIF630erm_01020/01021 genes (Fig. 3). Growth was efficiently rescued by homobetaine, proline betaine and DMSP, while all other tested compatible solutes (carnitine, glycine betaine, γ-butyrobetaine, crotonobetaine) provided salt stress protection in *B. subtilis* to a more moderate degree (Fig. 3) (Fig. S2).

In conclusion, the *C. difficile* CDIF630erm_01020/01021 operon clearly encodes a compatible solute transporter functional in *B. subtilis*, as system to which we like to refer in the following as OpuF. This ABC transporter preferentially transports homobetaine, proline betaine, DMSP, γ-butyrobetaine and glycine betaine. Our analysis could not show a function of the recombinant *C. difficile* CDIF630erm_03509/03510 operon in compatible solute uptake of *B. subtilis* under sustained salt stress growth conditions. This might indicate a different function for this *C. difficile* transporter or inefficient expression of the corresponding genes in the recombinant *B. subtilis* strain. However, the phenotypic behaviour of the *C. difficile opuF* mutant clearly excluded a role of this transporter encoding operon in high salt adaptation (see below).

The C. difficile *OpuF transporter confers high salt stress protection by importing compatible solutes in* C. difficile

Next, we proceeded to evaluate the physiological role of the OpuF transporter in *C. difficile*. For this purpose, we first generated an *opuFB* insertional mutant strain (Δ*opuFB*) in the *C. difficile* 630Δ*erm* genetic background using the ClosTron™ technology (Purdy *et al*., 2002; Heap *et al*., 2010). For unknown reasons, the *opuFB* mutant strain showed a delay in growth relative to its parent strain; however, it reached a final growth yield comparable to that of the wild type (Fig. 4). It was also more osmotically sensitive than the wild-type strain (Fig. 4).

We tested the salt stress-protective effects of eight compatible solutes for the *C. difficile* 630Δ*erm* wild-type strain and its *opuFB* mutant derivative for 24 h. With the exception of choline, all tested compatible solutes noticeably improved the growth of the *C. difficile* wild-type strain in the presence of 350 mM NaCl, while this was not the case for the *opuFB* mutant strain (Fig. 5). Hence, the OpuF ABC transporter is functional in *C. difficile* and serves as a compatible solute import system with a rather broad substrate specificity.

L-proline serves as a compatible solute for many bacteria but it can also function as a nutrient (Fichman *et al*., 2015). It was present in the MDM medium that we used for our experiments at a concentration of 9–12 mM (as determined by metabolomics). *Clostridioides difficile* can use both, L- and D-proline as a major energy substrate for the Stickland reaction (Neumann-Schaal *et al*., 2015; Hofmann *et al*., 2018). Thus, it did not serve as an effective osmostress protectant for this bacterium in the initial adaptation phase (24 h) to salt stress (Fig. 5). In agreement with this observation, an

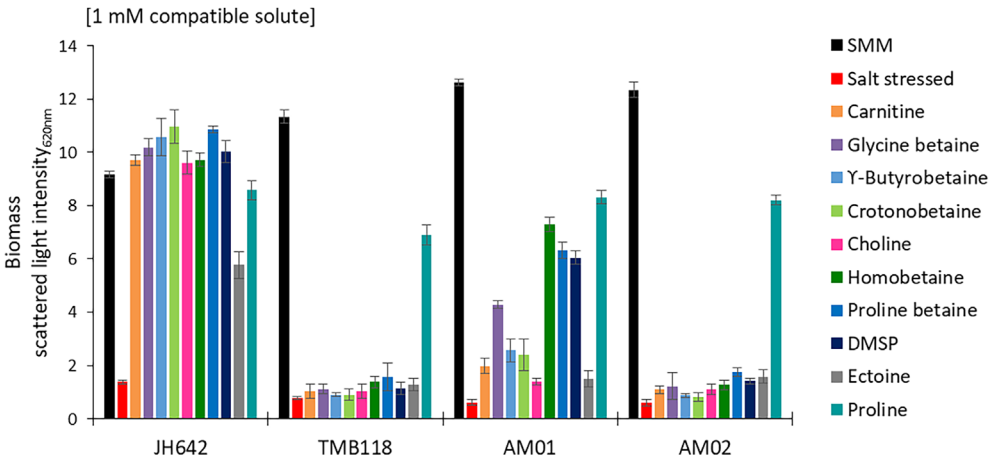

Fig. 3. CDIF630erm_01021 is a functional osmoprotectant uptake transporter. Growth of the *B. subtilis* wild type strain JH642, the compatible solute transporter-deficient *B. subtilis* strain TMB118, and TMB118 derivatives heterologously expressing the *C. difficile* OpuF transporter (CDIF630erm_01020/ CDIF630erm_01021) (strain AM01), or the *C. difficile* ABC transporter encoded by the CDIF630erm_03509/ CDIF630erm_03510 genes (strain AM02), was measured in the presence of 1 M NaCl with the addition of 1 mM of indicated compatible solutes (colour code in the right panel). Gain in biomass was determined by recording the intensities of scattered light (SLI) at 12 h, when the *B. subtilis* strain JH642 reached its SLI_{max} with salt stress addition in SMM medium supplemented with compatible solutes (coloured bars). In the *B. subtilis* strain TMB118, which lacks the four major compatible solute transporters OpuA to OpuD, the addition of compatible solutes had no beneficiary effect on its growth in the presence of 1 M NaCl. In case of strain AM01, higher SLIs values were reached in the presence of homobetaine, proline betaine, DMSP, γ-butyrobetaine, glycine betaine, crotonobetaine and carnitine. In contrast, strain AM02 failed to respond to the tested compounds. The wild type *B. subtilis* strain JH642, possessing all Opu transporters (OpuA to OpuE), was used as a positive control, and was able to utilize all tested compounds as osmolytes. Growth experiments were performed with at least four biological and three technical replicates. The standard deviation is given.

integration mutant in a potential proline transporter (CDIF630erm_03896, PutP homologue) failed to reveal any growth phenotype in the initial salt stress response (data not shown). However, proline plays a major role in the late response to salt stress (see below).

Compatible solutes recover salt stress-induced morphological changes of C. difficile

We used field emission scanning electron microscopy (FESEM) to observe the morphology of *C. difficile* cells grown in the absence or presence of salt stress. FESEM micrographs of both the wild type and of the Δ*opuFB* mutant revealed characteristic 2.8–6 μm long rods of *C. difficile* that had on average a cell width of 0.56 μm (Fig. 6A). In the culture of the Δ*opuFB* mutant, filamentous cells with a maximal length of up to 21 μm were observed (Fig. 6H). Strikingly, salt stress induced by the addition of 350 mM NaCl to the growth medium lead to the formation of coccoid cells with average diameters of 1.0–1.8 μm, and a smoother cell surface with no appendages such as flagella or pili (Fig. 6B and I). The impressive transition in cell morphology under salt stress conditions was observed both for the wild type and for the Δ*opuFB* mutant strain (Fig. 6B and I). We estimated the cell volume by measuring the dimensions of the rod-shaped wild type cells ($n = 18$) grown in the absence of salt stress, and those of the coccoid-shaped cells ($n = 20$) observed under growth conditions in which salt stress was imposed. We derived a cell volume of *C. difficile* of 0.7–1.5 μm^3 under growth conditions in which no salt stress was imposed, and a volume of 1.2–3.1 μm^3 when such unfavourable conditions were imposed.

Given the observed positive physiological effect caused by various compatible solutes on the salt tolerance of *C. difficile* (Fig. 5), we further characterized the impact of salt stress in the presence of different compatible solutes on the cell morphology. Wild type (wt) and the corresponding *opuFB* mutant strains were grown in the presence of 350 mM NaCl with and without 1 mM carnitine (Fig. 4), butyrobetaine, homobetaine, crotonobetaine and DMSP respectively, harvested at mid-exponential phase and analysed by FESEM. The NaCl-triggered drastic effects on cell morphology were largely reverted in the wild type strain when 1 mM of the various tested compatible solute was present in the growth medium (Fig. 6C–G). Differences in the protection efficiencies were observed. However, carnitine and the various betaines were found highly efficient (Fig. 6C–F). A lower degree of protection was observed when DMSP was added to the salt-stressed cells (Fig. 6G), thereby showing a mixture of coccoid- and rod-shaped cells. Overall, the compatible solute treated cells mainly kept their typical rod-like shape, whereas the *opuFB* mutant mainly retained its coccoid shape (Fig. 6J–N).

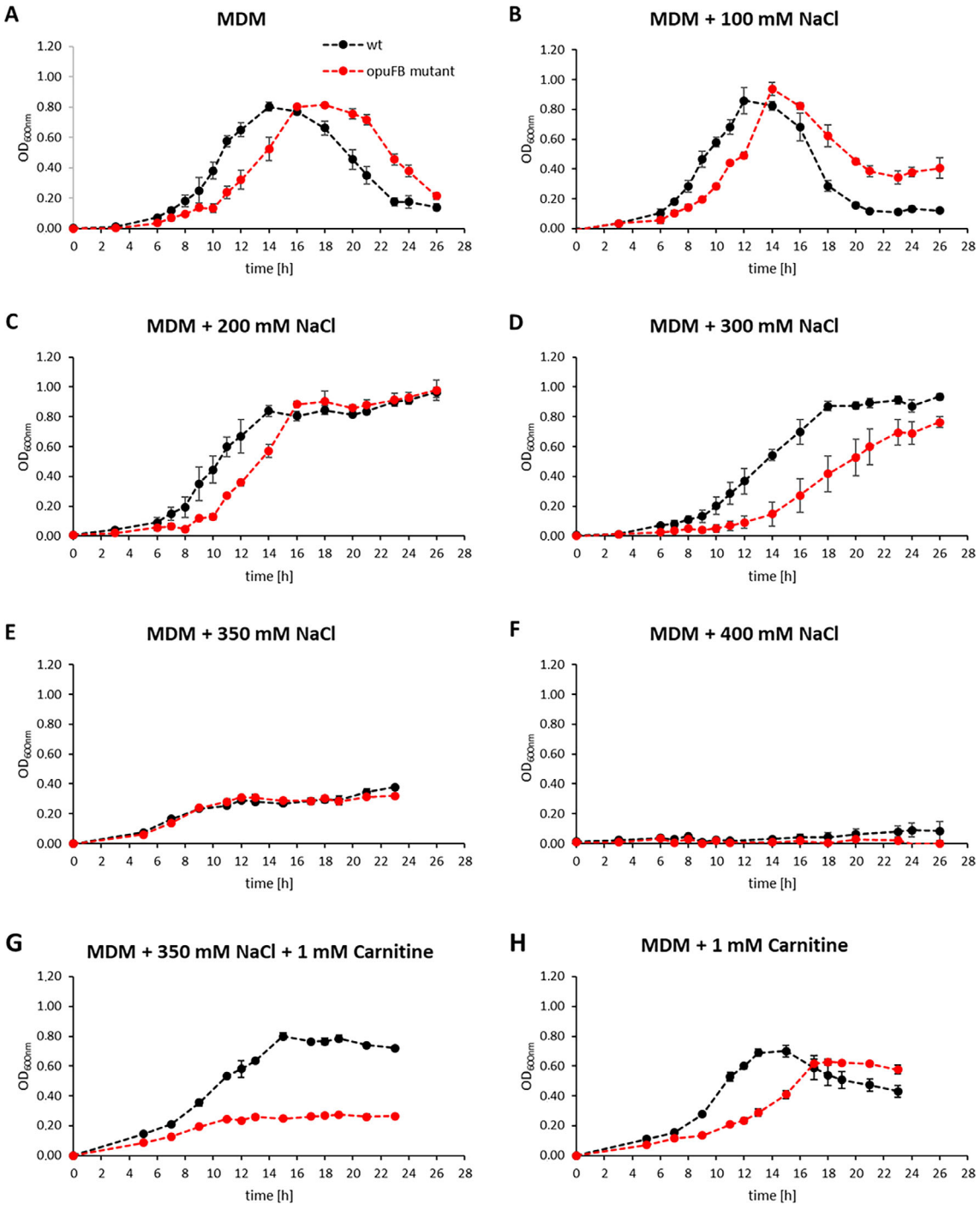

Fig. 4. Salt stress response of *C. difficile* 630Δ*erm opuFB* mutant. Salt tolerance of *C. difficile* 630Δ*erm* (black dotted lines) and its *opuFB* insertional mutant (red dotted lines) was compared by growing both strains in MDM (A), in MDM containing additionally 100 mM NaCl (B), 200 mM NaCl (C), 300 mM NaCl (D), 350 mM NaCl (E), 400 mM NaCl (F), 350 mM NaCl and 1 mM carnitine (G), and 1 mM carnitine (H). Growth of the cultures was recorded by monitoring the OD_{600nm}. Growth experiments were performed with at least four biological and three technical replicates. The standard deviation is given.

Salt stress inhibition of the C. difficile *energy metabolism is recovered by the presence of a compatible solute*

We also addressed the question to which extent salt stress impacts the metabolism of *C. difficile*. To gain insights into salt-induced metabolic changes, we characterized the extracellular and volatile fermentation profile of the wild type and the *opuFB* mutant strain under salt stress conditions in stationary phase and compared it to

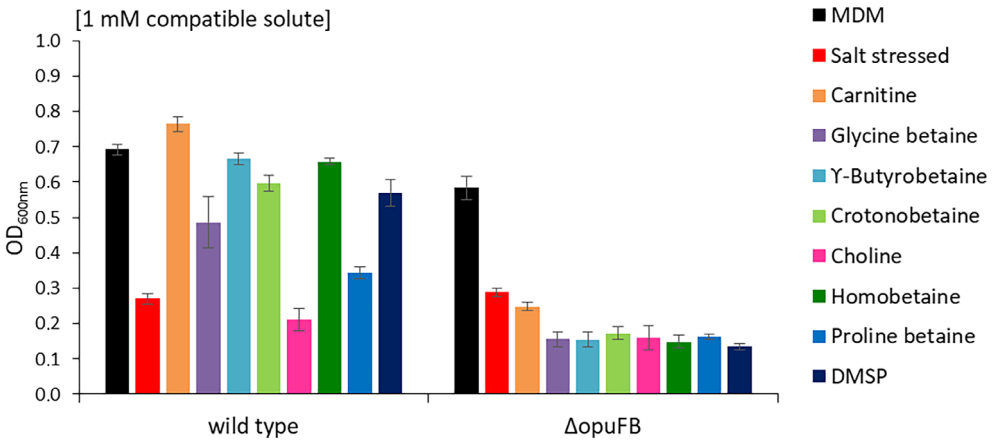

Fig. 5. Compatible solute spectrum of *C. difficile* 630Δ*erm* transported by OpuF. The influence of different compatible solutes at 1 mM final concentration (colour code on the right side) on the growth of salt-stressed *C. difficile* 630Δ*erm* and its *opuFB* mutant was monitored by measuring OD_{600nm} after 15 h, when the wild type reached its highest OD_{600nm} without osmotic stress (black bars). Salt stress was incurred through the addition of 350 mM NaCl to the medium. Growth experiments were performed with at least four biological and three technical replicates. The standard deviation is given.

unstressed reference controls (Fig. 7). Salt stress reduced the overall amounts of fermentation products in both strains. Most significant reductions were observed for acetate, propanoate and their oxidative Stickland fermentation products. This was also true for butanoate and isocaproate as reductive Stickland fermentation products. Interestingly, most alcohols were produced at similar concentrations under stressed and unstressed conditions. Importantly, the addition of carnitine to the growth medium of the wild type strain almost completely recovered the metabolite profile to the level of the unstressed control. In contrast, carnitine addition did not affect the metabolome of the *opuFB* mutant strain (Fig. 7), indicating that this compatible solute must be imported in order to exert the observed effects on the extracellular and volatile fermentation profile of the wild type *C. difficile* strain.

Next, we focused in more detail on the intra- and extracellular metabolic changes in the exponential growth phase of the wild type strain under salt stress conditions in the absence (Fig. 8A) and presence of carnitine (Fig. 8B). Salt stress decreased amino acid uptake and the secretion of alanine, and led to the reduced export of fermentation products while intermediates of the Stickland fermentation pathways were accumulated to higher levels in the cell. Proline and cysteine as highly preferred substrates for *C. difficile* (Neumann-Schaal *et al*., 2015; Hofmann *et al*., 2018) were consumed to a lower extent, and the corresponding fermentation products (acetate, 5-aminovalerate) were less abundant in the culture supernatant. The only fermentation product showing increased concentrations under salt stress with or without carnitine was lactate, which is commonly only observed in later growth phases and associated with the induction of toxin formation by *C. difficile* (Hofmann *et al*., 2021). In contrast, in the presence of carnitine, the metabolism was mostly reconstituted to a level of the unstressed condition, only few metabolites remained altered including the intermediates of the oxidative Stickland fermentation pathways and of glycolysis (Fig. 8B; Table S2). Notably, carnitine itself was not metabolized by the *C. difficile* cell, supporting its sole role as a metabolically inert compatible solute.

Short- and long-term adaptation of C. difficile *to salt stress*

Bioinformatic analyses revealed that the classical pathways of compatible solute production in bacteria including those for glycine betaine, ectoine and trehalose are absent in *C. difficile*. Thus, *C. difficile* seems not to react to salt stress like most other previously investigated bacteria through the biosynthesis of compatible solutes (Kempf and Bremer, 1998; Gunde-Cimerman *et al*., 2018). Consequently, metabolomic analyses of salt-stressed *C. difficile* (addition of 350 mM NaCl, logarithmic growth phase) failed to detect the accumulation of the classical compatible solutes (e.g. glycine betaine, trehalose, sucrose, glucosylglycerol or glycosylglycerate). Isoglutamate and glutamate as well as proline are detectable intracellularly but not accumulated under elevated salt concentrations. The employed method routinely detects μM amounts of these compounds. The most abundant potential compatible solute of *C. difficile* under unstressed growth conditions, isoglutamate, was even less prevalent under high salt conditions.

Extended growth experiment up to 60 h surprisingly revealed recovered growth of *C. difficile* in the presence of 350 mM NaCl after 25 h and at 400 mM NaCl after

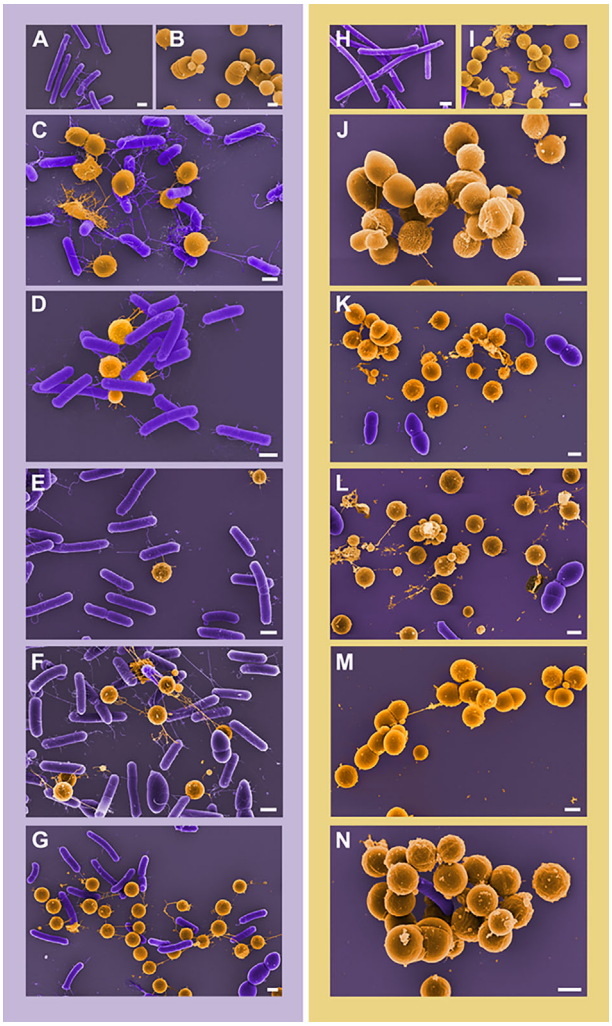

Fig. 6. Effect of salt stress on cell morphology. *Clostridioides difficile* 630Δ*erm* wild type (purple background) and its corresponding *opuFB* mutant (yellow background) grown in MDM (A, H), in MDM containing 350 mM NaCl (B, I), in MDM containing 350 mM NaCl and 1 mM carnitine (C, J), in MDM containing 350 mM NaCl and 1 mM Butyrobetaine (D, K), in MDM containing 350 mM NaCl and 1 mM Homobetaine (E, L), in MDM containing 350 mM NaCl and 1 mM Crotonobetaine (F, M), or in MDM containing 350 mM NaCl and 1 mM DMSP (G, N) were harvested at mid-exponential growth phase and analysed by FESEM. Bars represent 1 μm.

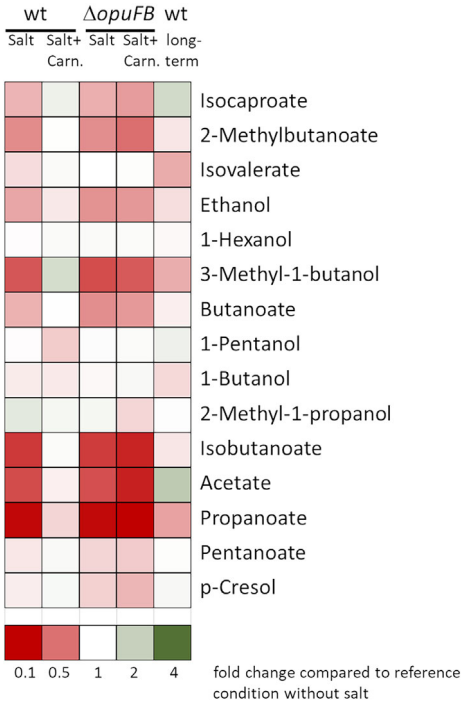

Fig. 7. Metabolic impact on the extracellular volatile fermentation products of *C. difficile* 630Δ*erm*. Shown are selected extracellular metabolites of the wild type (wt) and the Δ*opuFB* mutant strains as a heatmap in fold changes for the indicated fermentation products in presence of 350 mM NaCl (Salt) or 350 mM NaCl and 1 mM carnitine (Salt + Carn.) in comparison to unstressed conditions (column 1–4). The cells under salt-stressed conditions were grown to an OD_{600} of 0.28 (wt.) or 0.31 (Δ*opuFB* mutant) respectively. Cells in salt-containing medium supplemented with carnitine were grown to an OD_{600} of 0.77 (wt.) or 0.26 (Δ*opuFB* mutant). The right column represents the long-term adaptation of the wild-type to 400 mM NaCl over an extended incubation period of cells grown to an OD_{600} of 0.3. Less abundant products are labelled in red; more abundant products are labelled in green. All experiments are based on five or four (long-term adaptation) independent cultivations of the respective strains.

35 h (Fig. 9). In order to understand the metabolic basis for these observations, we first monitored the volatile fermentation products of *C. difficile* (Fig. 7, right column) and observed the alterations in the fermentation profile which showed elevated levels of isocaproate and acetate and a reduced level of isovalerate and propanoate. This indicates that leucine and threonine as substrates are redirected to reductive pathways (reducing equivalent sinks) instead of oxidative pathways (ATP formation by substrate-level phosphorylation). Consequently, we compared the major non-volatile intracellular metabolites of cultures harvested at $OD_{0.5max}$ in MDM compared to MDM supplemented with 400 mM NaCl. We detected a 5.1-fold increase of the intracellular proline concentration which was accompanied by the lower abundance of leucine and leucine fermentation intermediates (2-oxoisocaproate and 2-hydroxyisocaproate) and the rearrangement of the threonine metabolism (Fig. 8C) already indicated by the fermentation profile. 2-oxobutanoate and the side product 2-aminobutanoate were less abundant which are representative for the oxidative pathway to propanoate. In contrast, glycine was found in higher concentrations in the cell. Thus, the second metabolic route of the threonine metabolism via the glycine reductase complex was employed. However, *C. difficile* seemingly rearranges its reductive energy metabolism to allow proline accumulation in the cell. Under the reference conditions, proline is the favoured reductive

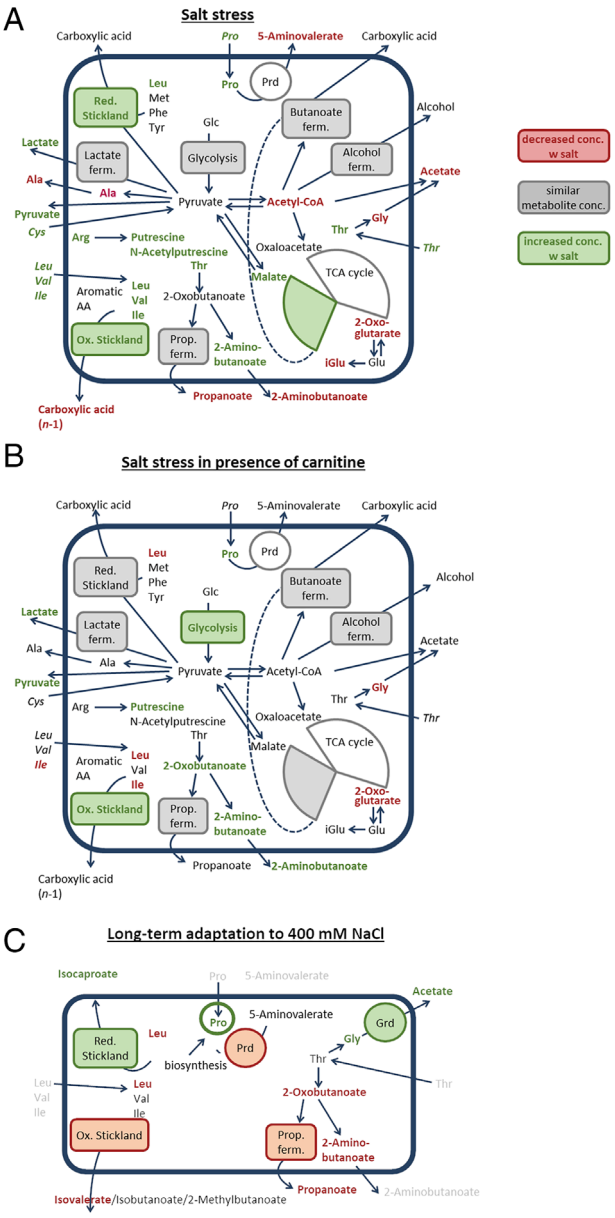

Fig. 8. Overview of adaptation of metabolism in *C. difficile* under salt stress conditions. Shown are metabolomics data obtained for *C. difficile* wild type grown in the exponential phase (OD_{600} of about 0.55 in MDM and MDM supplemented with carnitine or 0.24 in MDM with NaCl respectively) (A) comparing salt-stressed bacteria (350 mM NaCl) to unstressed bacteria and (B) salt-stressed bacteria grown in the presence of 1 mM carnitine with the unstressed bacteria. (C) A limited set of the most abundant intracellular metabolites and the volatile fermentation products was analysed for the long-term adaptation. Metabolomic data are represented by the metabolite names and the pathway boxes, generally increased concentrations are shown in green, while decreased concentrations are depicted in red (fold change >1.5). Metabolites in light grey were not analysed in the long-term adaptation experiment. All experiments are based on five or four (long-term adaption) independent cultivations of the wild type strain.

substrate likely due to the coupling of the proline reductase to the RNF complex. In turn, accumulated proline can act as a compatible solute and thereby probably allowed for the recovery of growth. Notably, major metabolic rearrangements of the energy metabolism are required to provide the salt-stressed *C. difficile* cell with the compatible solute L-proline.

Discussion

A microbiome dysbiosis induced by treatment with broad-spectrum antibiotics is a pre-condition leading to the development of severe *C. difficile* infections in humans (Jenior *et al*., 2017). This goes hand in hand with the perturbance of the bile acid composition and the overall metabolic profile of the infected host, both of which favour *C. difficile* spore germination and subsequent growth of vegetative and toxin-producing cells (Theriot *et al*., 2014; Buffie *et al*., 2015; Robinson *et al*., 2019). Once these conditions are established, salt stress is one of the major extracellular factors that vegetative cells need to cope with in the human intestine (Overduin *et al*., 2014). Here, we have focused on the initial and long-term cellular responses of *C. difficile* to sustained salt stress. Cellular responses to high salinity surroundings are key contributors to the ability of pathogens to conquer and persist in infected hosts and to survive osmotically harsh environmental conditions when they leave their preferred hosts (Sleator and Hill, 2001; Casey and Sleator, 2021; Gregory and Boyd, 2021).

The prevailing osmolarity in the human intestine corresponds to a salinity of about 350 mM NaCl (Chowdhury *et al*., 1996; Overduin *et al*., 2014). High concentrations of sugars would also increase the osmolarity in the gut but such conditions are unlikely to prevail due to the high metabolic activities of the dense microbiome (Halmos *et al*., 2015). As a matter of fact, accumulation of saccharides as the result of disease leads to an increased osmotic load and causes symptoms of intestinal distention, rapid peristalsis and diarrhoea (Robayo-Torres *et al*., 2006). Thus, we focused our attention on the salt stress that *C. difficile* will inevitably experience in its main ecophysiological niche, the gut. Our data do not allow us to distinguish between true osmotic stress responses of *C. difficile* and those that are incurred by the ionic nature of the added salt (NaCl). We consider it however likely, that the data reported here reflect both ionic and osmotic effects on metabolism, growth and cell morphology. Clearly, further studies are required to distinguish true osmotic from salt-elicited effects.

Long-term (after approx. 24 h) salt-stressed *C. difficile* cells are capable of rearranging its reductive metabolic energy generation pathways to allow the accumulation of L-proline, a well-known compatible solute, in the cell. This is achieved by using higher shares of leucine as reductive substrate and by shifting the threonine metabolism from the oxidative pathway via 2-oxobutanoate to glycine

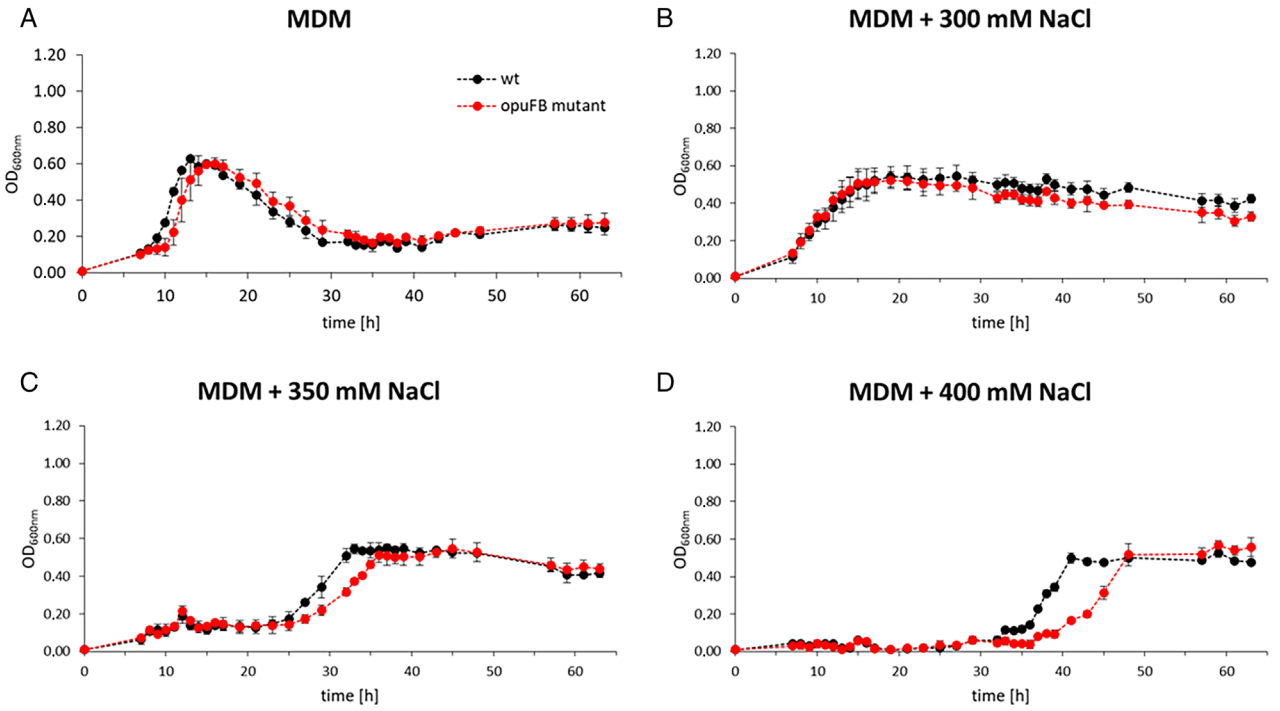

Fig. 9. Long-term salt stress response of *C. difficile* 630Δ*erm opuFB* mutant. Salt tolerance of *C. difficile* 630D*erm* (black dotted lines) and its *opuFB* insertional mutant (red dotted lines) was compared by growing both strains in MDM (A), MDM with 300 mM NaCl (B), 350 mM NaCl (C), and 400 mM NaCl (D). Growth of the cultures was recorded by monitoring the OD_{600nm} over 63 h. Growth experiments were performed with at least four biological and three technical replicates. The standard deviation is given.

as an intermediate using now the glycine reductase complex. The rearrangement of the complex balance between oxidative and reductive fermentation reflects the high metabolic flexibility of this pathogen to adapt to altering conditions in the human gut. Overall, this long-term adaptation reaction seems to represents a rearrangement of the metabolism of the cells and might not necessarily reflect a salt-induced synthesis of a compatible solute.

The level of osmolarity/salinity in the intestine is variable and depends on the diet (Fordtran and Locklear, 1966). The degree of salinity (350 mM NaCl) that we imposed under laboratory conditions onto *C. difficile* cells represent a threshold value where a reasonable level of growth is still possible, while an increase by just 50 mM NaCl prevents growth altogether for almost 20 h before the long-term adaptation reaction via metabolic rearrangements kicks in (Fig. 4C). Seemingly, *C. difficile* does not possess a substantial physiological buffer to safeguard its growth under high salt conditions that even marginally exceed (Fig. 4) those prevailing in the gut.

As in other microorganisms, the cellular adaptation of *C. difficile* to sustained salt stress will in all likelihood involve the import of potassium ions (Wood, 2011; Bremer and Krämer, 2019). As evidence from the *C. difficile* genome sequence, this anaerobic bacterium lacks the ability to produce compatible solutes that are typically synthesized in members of the *Bacteria* (e.g. glycine betaine, ectoine, trehalose) (da Costa *et al*., 1998; Kempf and Bremer, 1998; Gunde-Cimerman *et al*., 2018). Hence, both genomic data and our metabolome analysis show that the second arm of the *salt-out* adjustment response, the synthesis of compatible solutes, is missing in *C. difficile* during the initial adaptation phase in the first 24 h. With its initial weak salt tolerance of 350 mM NaCl, *C. difficile* is exclusively relying on the presence of externally provided compatible solutes to adjust to unfavourable salt-stress incurred growth conditions. Various types of compatible solutes (e.g. carnitine and glycine betaine) are present in food sources and their import (tested at 1 mM concentration in our study) restored the growth of salt-stressed *C. difficile* cells. Compatible solutes are naturally present in the higher micromolar to lower millimolar range in the gut in dependence of food intake (Craig, 2004; Koeth *et al*., 2014; Simó and García-Cañas, 2020; Day-Walsh *et al*., 2021). High-affinity transporters are thus required for their acquisition.

The adjustment of *C. difficile* to persistent salt stress resembles that of a *B. subtilis* mutant which can import potassium ions but lacks the enzymes for the synthesis of the only compatible solute this non-pathogenic soil bacterium can produce *de novo*, L-proline (Brill

et al., 2011). As a consequence, such a *B*. *subtilis* strain cannot effectively withstand osmotic or salt stress (Hoffmann and Bremer, 2016, 2017), and like the natural situation for *C*. *difficile*, results in a rather salt-sensitive growth phenotype (Brill *et al*., 2011). Collectively, our data reveal that the ability of *C*. *difficile* to cope with salt stress is restricted to a level that just about matches the degree of salt in the mammalian intestine (Chowdhury *et al*., 1996; Overduin *et al*., 2014). Although the proficiency to synthesize compatible solutes is certainly not the only determinant to attain a substantial degree of osmostress tolerance (Wood, 2011; Bremer and Krämer, 2019), it clearly is a key contributor to this process in many bacteria (Kempf and Bremer, 1998; Gunde-Cimerman *et al*., 2018). As *C*. *difficile* seemingly lacks this important physiological trait, the sensitivity of this intestinal pathogen to salt stress (Fig. 4) becomes now understandable.

While *C*. *difficile* cannot synthesize compatible solutes when it is initially exposed to salt stress, it nevertheless makes use of these stress-relieving compounds through import. It uses for this purpose an OpuF-type uptake system (Teichmann *et al*., 2018) which belongs to a subgroup of binding-protein-dependent ABC-transporters in which the substrate-binding domain is fused to the transmembrane domain (Sikkema *et al*., 2020). Our modelling study indicates that the OpuFB substrate-binding domain of the *C*. *difficile* OpuF transporter resembles in its overall fold that of ligand-binding proteins of canonical ABC transporters (Berntsson *et al*., 2010). The model also revealed the presence of an aromatic cage in the OpuFB ligand-binding domain which architecturally resembles that found in many substrate-binding proteins with specificity for compatible solutes (Schiefner *et al*., 2004; Horn *et al*., 2006; Oswald *et al*., 2008; Du *et al*., 2011; Pittelkow *et al*., 2011; Sikkema *et al*., 2020). The import of all compatible solutes tested in our study was attributable to the OpuF ABC transport system.

Clostridioides difficile possesses genes for a second OpuF-type ABC transporter but there is currently no evidence from our data for its involvement in the acquisition of compatible solutes, despite that the substrate-binding domain possesses the characteristic aromatic cage as well (Fig. 2). However, there is precedent for this situation, as the BilE substrate-binding protein from *L*. *monocytogenes* (Ruiz *et al*., 2016) and the YehZ substrate-binding protein from *Brucella abortus* (Herrou *et al*., 2017) possess OpuFB-type substrate-binding pockets with *aromatic cages*. Yet, there is no evidence that these proteins can bind compatible solutes (Ruiz *et al*., 2016; Herrou *et al*., 2017).

The most amazing finding of our study is the observation of a striking morphological change in which *C*. *difficile* switches from its typical rod-like shape to a coccoid form under salt stress conditions (Fig. 6B). Importantly, this shift in cell morphology is reversible in an OpuF-dependent fashion with several tested compatible solutes (Fig. 6). It is, for instance, known that the compatible solute glycine betaine can reverse the osmotic stress-incurred increase in the cell size of *S*. *aureus* and corresponding changes in the architecture of the peptidoglycan (Vijaranakul *et al*., 1995, 1997). However, to the best of our knowledge, morphological changes of the type that we describe here for *C*. *difficile* have never been observed before in microorganisms exposed to sustained osmotic/salt stress. Whether the transition from a rod-shape to a coccoid cell form represents a salt stress adaptive cellular reaction of *C*. *difficile*, or whether it simply reflects a sensitivity of cell-wall biosynthetic enzymes to changes in intracellular ionic and crowding conditions (van den Berg *et al*., 2017), remains to be seen. Collectively, our data suggest that the OpuF-mediated import of various compatible solutes play an important role for *C*. *difficile* to physiologically counteract environmentally imposed salt stress.

Experimental procedures

Chemicals and reagents

All antibiotics, amino acids and compatible solutes used were from laboratory stocks or were purchased from Sigma-Aldrich (Taufkirchen, Germany) if not stated otherwise. Casamino acids were obtained from Carl Roth GmbH (Karlsruhe, Germany).

Bacterial strains, media and growth conditions

The strains that were used in this study are listed in Table 1. *Escherichia coli* and *B*. *subtilis* strains were routinely cultivated at 37°C in lysogenic broth (LB) at 180 rpm under aerobic conditions. Media were supplemented with ampicillin (100 μg ml^{-1}) or chloramphenicol (*E*. *coli*: 20 μg ml^{-1}, *B*. *subtilis*: 5 μg ml^{-1}) if required. Transport studies in *B*. *subtilis* were performed in Spizizen minimal medium (SMM) supplemented with a trace element solution and 0.5% (wt./vol.) glucose as a carbon source (Harwood and Archibald, 1990). L-tryptophan (20 μg ml^{-1}) and L-phenylalanine (18 μg ml^{-1}) were added to SMM as *B*. *subtilis* JH642 and its derivatives are auxotrophic for these amino acids (Brehm *et al*., 1973). *Clostridioides difficile* 630Δ*erm* (obtained from the DSMZ, Braunschweig/Germany) (Dannheim *et al*., 2017) and its isogenic *opuFB* insertional mutant (hereafter referred to as Δ*opuFB*) were routinely grown without shaking at 37°C in an anaerobic chamber from Coy Laboratories (Grass Lake, MI, USA) with an atmosphere of 95% N_2 and 5% H_2. For routine cultivation,

Brain-Heart-Infusion (BHI) broth or BHI-agar (Sigma-Aldrich) supplemented with 0.1% (wt./vol.) L-cysteine and 5 g L^{-1} yeast extract yielding BHIS were used. *Clostridioides difficile* supplement (Sigma Aldrich) containing D-cycloserine (500 μg ml^{-1}) as well as cefoxitin (16 μg ml^{-1}), thiamphenicol (15 μg ml^{-1}) and erythromycin (2.5 μg ml^{-1}) were used during mutagenesis experiments. The composition of the defined minimal medium for *C. difficile* MDM is given in Table S1. All growth experiments were performed with at least four biological and three technical replicates.

Construction of C. difficile *630Δ*erm opuFB *mutant*

A *C. difficile* 630Δ*erm opuFB* insertional mutant was generated using the ClosTron system based on the stable insertion of a group II intron into the gene of interest. For this procedure, the shuttle vector pMTL007C_E2 was designed with a specific intron targeting region using the Perutka algorithm (Perutka *et al*., 2004) implemented at the ClosTron website (http://www.clostron.com). The customized vector pMTL007C-E2::Cdi_opuFB-936I937s was purchased from ATUM (Newark, CA, USA), and introduced into mating competent *E. coli* CA434 cells via transformation. Transfer of this plasmid to wild type *C. difficile* 630Δ*erm* cells was carried out as described previously (Purdy *et al*., 2002; Heap *et al*., 2010). Transformants were selected on BHI agar containing 500 μg ml^{-1} D-cycloserine and 16 μg ml^{-1} cefoxitin (*C. difficile* supplement, Sigma-Aldrich) and 15 μg ml^{-1} thiamphenicol (Sigma-Aldrich). After 72 h of anaerobic culturing at 37°C, mutant selection was performed on BHI agar containing *C. difficile* supplement and 2.5 μg ml^{-1} erythromycin. Homologous recombination leading to target gene disruption (Δ*opuFB*) was confirmed by PCR using primers specific for the type II intron and the *opuFB* locus (Table 2).

Table 2. Primers used in this study.

Primer	Sequence (5′ → 3′)	Reference
ClosTron mutagenesis EBS_universal	CGA AAT TAG AAA CTT GCG TTC AGT AAA C	Heap *et al*. (2007)
ErmRAM_Fw	ACG CGT TAT ATT GAT AAA AAT AAT AGT GGG	Heap *et al*. (2007)
ErmRAM_Rv	ACG CGT GCG ACT CAT AGA ATT ATT TCC TCC CG	Heap *et al*. (2007)
Cdi_opuFB_Fw2	GTA AAA TTG AAG TTG CAG TTA C	This work
Cdi_opuFB_Rv1	CCA AGT TCA TCC ACT TGA TAG T	This work
Bacillus mutagenesis		
pX_universal_Fw	GGC GCT CAG GAT CTG TTA AGA TC	This work
pX_universal_Rv	CGA TAA GCT TCT AGG ATC TCG AGC	This work
Bsub_Promotor_Fw	AGC TGA TCA TCC CTT CAA ATG GC	This work
OpuFA_opt_Fw1	ATG ATT GAA ATT AGA AAT GTC ACG AAA AAA ATC	This work
OpuFB_opt-Fw2	GCA CGG AAT GGC AAA CTT TTT TAA C	This work
OpuFA_opt_Fw3	GGT TGA AAT CCT GAA TGT CAT GAA TAG AAA TAG	This work
OpuFA_opt_Rv1	GTT TAG CCC AGG ACT GAA ACT TC	This work
OpuFB_opt_Rv2	CCA GGC CTT CTT TAA CCA GAA ATG	This work
unkn. Transp_opt_F2	GAA TGA CAC CGA TTA TTC AGT TCA AG	This work
unkn_Transp_Fw3	CGC AAC AAA GCC GAT GAC AG	This work

Generation of B. subtilis *strains carrying* C. difficile *transporter genes*

The operons encoding the OpuF transporter (CDIF630erm_01020, CDIF630erm_01021) and a putative ABC-type glycine/betaine transport system (CDIF630erm_03509, CDIF630erm_03510, hereafter abbreviated as UtS ('unknown transporter system') of *C. difficile* 630Δ*erm* were fused with the natural promoter region including the ribosomal binding site (RBS) of the *B. subtilis opuC* operon (Kappes *et al*., 1999). Furthermore, the intergenic RBS was replaced by its *B. subtilis* counterpart (Fig. S2). The codon usage of the *C. difficile* 630Δ*erm* OpuF and UtS transporters were optimized for *B. subtilis* using the GeneArt Gene Synthesis tool of Thermo Fisher Scientific. Sequences were synthesized as shuttle vectors pMA-RQ-$opuF_{Cdiff}$ and pMA-RQ-utS_{Cdiff}, and purchased from Thermo Scientific (Table 3). The $opuF_{Cdiff}$ and utS_{Cdiff} DNA-fragments respectively were excised with XbaI (New England BioLabs®, Frankfurt am Main, Germany), and were inserted into plasmid pX, which was cleaved with the same enzyme, thereby replacing the *xylR*-gene and the P_{xylA}-promoter of the pX-vector backbone (Kim *et al*., 1996). In the resulting plasmids pXΔ*xylR*::$opuF_{Cdiff}$ and pXΔ*xylR*::utS_{Cdiff}, the respective operon is flanked by segments of the 5′ and 3′ sequences of the *amyE* thereby allowing homologous recombination into the non-essential chromosomal *amyE* gene of the *B. subtilis* strain TMB118 as a single copy. In strain TMB118 the operons encoding the OpuA, OpuB, OpuC and OpuD osmoprotectant uptake systems are deleted. Only the proline-specific OpuE transporter is present because it is essential for the proline release and

Table 3. Vectors and plasmids used in this study.

Name	Features	Reference
pMA-RQ-opuF$_{C.\ difficile\ 630\Delta erm}$	Amp^R, Col E1 origin, optimized *CDIF630erm_01020*::*CDIF630erm_01021* operon, *B. subtilis* promoter region	This work (Thermo Fisher Scientific, Waltham, USA)
pX	*xyl*R, Cm^R, Amp^R *amyE* front/back	Kim *et al*. (1996)
pXΔ*xylR*::*opuF*$_{C.\ difficile\ 630\Delta erm}$	Cm^R, Amp^R, Δ*xylR*, optimized *opuF*$_{C.\ difficile\ 630\Delta erm}$ (*CDIF630erm_01020*::*CDIF630erm_01021*; annotated as *opuCA* and *opuCC* respectively) inserted	This work
pMTL007C-E2::Cdi_*opuFB*-936 I 937s	pMTL007C-E2 retargeted to *C. difficile* 630Δ*erm*-*opuFB*936I937s:: intron *ermB*	This work (ATUM)

recapturing cycle in *B. subtilis* (Hoffmann *et al*., 2012). As a result, this *B. subtilis* mutant cannot be protected from osmotic stress by externally provided compatible solutes, except by L-proline (Teichmann *et al*., 2017). Successful cloning was confirmed by DNA sequencing with plasmid and insert specific primers (Table 2). Naturally competent *B. subtilis* TMB118 cells were transformed with the respective plasmid. Resulting transformants were selected on LB-agar with chloramphenicol. Homologous recombination into the *amyE* locus was verified by checking for *amyE* dependent amylase activity (Brill *et al*., 2011). Amylase negative clones, designated AM01 and AM02 harbouring *opuF*$_{Cdiff}$ and *utS*$_{Cdiff}$ respectively, were used for detailed transport studies.

Transport assays in B. subtilis

Transport assays were performed with slight modifications as previously described (Teichmann *et al*., 2017, 2018). Briefly, *B. subtilis* strains were cultured at 37°C in SMM with 0.5% (wt./vol.) glucose as the carbon and energy source. Pre-cultures that were grown to exponential growth phase in 20 ml SMM in 100 ml Erlenmeyer flasks were diluted to an optical density at a wavelength of 578 nm (OD_{578}) of 0.1 in fresh SMM. A 1 ml-aliquot of this suspension was transferred into the wells of 48-well FlowerPlates MTP-48-B (m2p-labs GmbH, Baesweiler, Germany). Bacteria were grown in a BioLector mini bioreactor system (m2p-labs GmbH) for 25 h at 37°C and 1400 rpm under humidity control. The gain in biomass was derived from the intensity of the scattered light at 620 nm (scattered light index, SLI) at a gain of 10. Hyperosmotic stress was imposed onto the *B. subtilis* cells by the addition of NaCl to a final concentration of 1 M from a 5 M stock solution. Compatible solutes were added to cultures at a final concentration of 1 mM from sterile-filtered 100 mM stock solutions prepared in ddH_2O.

Growth and salt stress protection assays in C. difficile

Growth assays of *C. difficile* 630Δ*erm* and its isogenic Δ*opuFB* mutant were performed in a minimal defined medium (MDM) as published previously (Neumann-Schaal *et al*., 2015). To improve the biomass yield for subsequent analyses, L-threonine was included at 0.563 g L^{-1}. Pre-cultures were prepared in *C. difficile* minimal medium (CDMM) with minor modifications to a previously described recipe (Neumann-Schaal *et al*., 2015): NaH_2PO_4 was added to a final concentration of 14.5 mM; the concentrations of glucose and D-biotin were adjusted to 10 and 0.003 g L^{-1} respectively. Bacteria grown on chromID® plates were used to inoculate CDMM. Two sequential pre-cultures were prepared, in order to reduce the spore load in the final culture. After growing the first pre-culture for 20 h, the second pre-culture was inoculated with a 1:100 dilution and grown to an OD_{600} of 0.6. Next, the main cultures for the growth experiments were inoculated from this second pre-culture to an initial OD_{600} of 0.01 in a final volume of 10 ml MDM. Growth was monitored by measuring the OD_{600} over 26 h. Hyperosmotic stress was induced by supplementing the main cultures with increasing concentrations of NaCl from a 5 M stock solution. In order to test the salt stress-protective activity of different compatible solutes, bacteria were grown in the presence of 350 mM NaCl with or without 1 mM of the respective compatible solute.

Genome-wide search for compatible solute biosynthetic genes in C. difficile *630*Δerm

We searched the genome sequence of *C. difficile* 630Δ*erm* (Dannheim *et al*., 2017) (genome identification number 2871977330) deposited at the Joint Genomic Institute Integrated Microbial Genomes and Microbiomes (JGI/IMG/MER) database for genes encoding glycine betaine, ectoine and trehalose, widely used compatible solutes in bacteria (Kempf and Bremer, 1998). To assess the presence of genes for the synthesis of glycine betaine from the precursor choline, we used the proteins encoded by the *Escherichia coli betBA* (gene identification numbers CAD6021196.1 and CAD6021202.1 respectively) and the *Bacillus subtilis gbsAB* genes (gene identification numbers NP_390984.1 and NP_390983.2 respectively) as search queries. No BetBA/

GbsAB-type proteins were found. The ectoine biosynthetic genes (*ectABC*) are typically organized in an operon and the *ectC*-encoded ectoine synthase is the signature enzyme for ectoine production. Likewise, using the EctC proteins from *Halomonas elongata* and from *Virgibacillus pantothenticus* as search queries (gene identification numbers AAC15883.1 and AAS93808.1 respectively), no *ect* biosynthetic gene cluster was present in the genome of *C. difficile* 630Δ*erm*. The compatible solute trehalose can be synthesized by various types of enzymes. No genes for the synthesis of trehalose were detected in *C. difficile* 630Δ*erm* when the proteins of the *otsAB*-encoded genes from *E. coli* (gene identification numbers BAA15717.1 and BAA15718.1 respectively), of the *treYZ*-encoded genes from *Pseudomonas aeruginosa* (gene identification numbers KFL05971.1 and PWU33707.1 respectively), or that of the *treS*-encoded gene from *Mycobacterium tuberculosis* (gene identification number CCE35668.1) were used as the search queries.

Field emission scanning microscopy

Clostridioides difficile 630Δ*erm* was cultivated anaerobically in MDM with and without additional 350 mM NaCl in presence or absence of 1 mM of the indicated compatible solute. A volume of 20 ml cell culture was harvested at mid-exponential phase and pre-fixed with 1% (wt./vol.) formaldehyde followed by fixation with 5% (wt./vol.) formaldehyde and 2% (vol./vol.) glutaraldehyde. Further sample preparation was carried out as described previously (Berges *et al*., 2018) with minor modifications. The FESEM examinations were performed with a Zeiss Merlin microscope (Oberkochen, Germany) equipped with an Everhart-Thornley SE-detector and an Inlens SE-detector in a 75:25 ratio with an acceleration voltage of 5 kV.

Metabolome studies

All metabolites analysed in this study are listed in Tables 2 and 3. Samples for metabolomic studies were collected during the mid-exponential phase from five (major experiment) or four (additional experiment for long-term adaptation) independent biological replicates cultivated in MDM and their modified variants. Cultures were harvested under anaerobic conditions and were transferred into gas-tight polypropylene tubes (TPP, Trasadingen, Switzerland). Sampling conditions were chosen as described previously (Hofmann *et al*., 2018), unless stated otherwise. Samples for fermentation profiling were collected at OD_{max}, and the bacteria were pelleted by centrifugation (8000 rpm for 10 min at 4°C). 1 ml aliquots of the supernatants were transferred to cryotubes for fermentation analysis. Cell pellets and supernatants were immediately frozen in liquid nitrogen and stored at −80°C. GC/MS was used for the detection and quantification of intra- and extracellular as well as volatile compounds and for major non-volatile intracellular compounds in the long-term adaptation experiment. The measurements were performed on an Agilent GC-MSD system (7890B coupled to a 5977 GC) equipped with a high-efficiency source and a PAL RTC system as described before (Will *et al*., 2019). The samples were prepared and extracted as previously described with minor modifications (Hofmann *et al*., 2018). For the long-term adaptation experiment, the samples were only analysed in split mode. For the analysis of intra- and extracellular compounds, 150 µl of the polar phase were transferred into glass vials. For volatile compounds an Agilent VF-WAXms column (0.25 mm 30 m, Agilent, Santa Clara, CA, USA) was integrated into the system, and a volume of 1 µl was injected in pulsed split mode with a split ratio of 10:1 (split flow of 12 ml min^{-1}). Separation and measurement were conducted as described before (Neumann-Schaal *et al*., 2015). LC/MS was deployed for the analysis of coenzyme A (CoA) derivatives and amino acids. For this purpose, frozen precipitated cells were re-suspended in 700 µl methanol per 1 mg dry weight. A volume of 1 ml cell suspension was transferred into 2 ml screw-cap tubes containing 600 mg glass beads (70–110 µM diameter). As an internal standard 250 ng of $^{13}C_3$-malonyl-CoA was added, and the cells were lysed using a FastPrep-24 classic instrument equipped with a CoolPrep adapter (MP Biomedicals, Stadt. Land). The lysate was mixed with 10 ml ice-cold ammonium acetate (25 mM, pH 6) and centrifuged subsequently (5 min, 10 000 rpm, 4°C). The extraction of CoA derivatives was performed using a Strata XL-AW solid-phase column (Phenomenex, Aschaffenburg, Germany) as described previously (Wolf *et al*., 2016). The measurement was carried out on an Agilent LC-QTOF system (6545 coupled to a 1290 Infinity II UHPLC) equipped with an electrospray interface. The separation was driven on a C_{18} analytical column (Gemini 2.0 × 150 mm, particle size 3 mm; Phenomenex) followed by data analysis as described previously (Wolf *et al*., 2016). Samples for amino acid analysis were prepared and measured with a 1260 Infinity II HPLC system as previously described (Hofmann *et al*., 2018).

Acknowledgements

This work was funded by the Federal State of Lower Saxony, Niedersächsisches Vorab CDiff and CDInfect projects (VWZN2889/3215/3266). The authors would like to thank Gesa Martens and Ina Schleicher for their outstanding technical assistance. E.B. is grateful to Gert Bange and Anke

Becker (both at SYNMIKRO, University of Marburg) for their kind hospitality and support.

References

Abt, M.C., McKenney, P.T., and Pamer, E.G. (2016) *Clostridium difficile* colitis: pathogenesis and host defence. *Nat Rev Microbiol* **14**: 609–620.

Bartlett, J.G., Onderdonk, A.B., Cisneros, R.L., and Kasper, D.L. (1977) Clindamycin-associated colitis due to a toxin-producing species of *Clostridium* in hamsters. *J Infect Dis* **136**: 701–705.

Berges, M., Michel, A.-M., Lassek, C., Nuss, A.M., Beckstette, M., Dersch, P., *et al*. (2018) Iron regulation in *Clostridioides difficile*. *Front Microbiol* **9**: 3183.

Berntsson, R.P.A., Smits, S.H.J., Schmitt, L., Slotboom, D.J., and Poolman, B. (2010) A structural classification of substrate-binding proteins. *FEBS Lett* **584**: 2606–2617.

Brehm, S.P., Staal, S.P., and Hoch, J.A. (1973) Phenotypes of pleiotropic-negative sporulation mutants of *Bacillus subtilis*. *J Bacteriol* **115**: 1063–1070.

Bremer, E., and Krämer, R. (2019) Responses of microorganisms to osmotic stress. *Annu Rev Microbiol* **73**: 313–334.

Brill, J., Hoffmann, T., Bleisteiner, M., and Bremer, E. (2011) Osmotically controlled synthesis of the compatible solute proline is critical for cellular defense of *Bacillus subtilis* against high osmolarity. *J Bacteriol* **193**: 5335–5346.

Britton, R.A., and Young, V.B. (2014) Role of the intestinal microbiota in resistance to colonization by *Clostridium difficile*. *Gastroenterology* **146**: 1547–1553.

Buffie, C.G., Bucci, V., Stein, R.R., McKenney, P.T., Ling, L., Gobourne, A., *et al*. (2015) Precision microbiome reconstitution restores bile acid mediated resistance to *Clostridium difficile*. *Nature* **517**: 205–208.

Casey, D., and Sleator, R.D. (2021) A genomic analysis of osmotolerance in *Staphylococcus aureus*. *Gene* **767**: 145268.

Chowdhury, R., Sahu, G.K., and Das, J. (1996) Stress response in pathogenic bacteria. *J Biosci* **21**: 149–160.

Craig, S.A.S. (2004) Betaine in human nutrition. *Am J Clin Nutr* **80**: 539–549.

da Costa, M.S., Santos, H., and Galinski, E.A. (1998) An overview of the role and diversity of compatible solutes in bacteria and archaea. In *Advances in Biochemical Engineering/Biotechnology*, pp. 117–153. London, UK: Springer Nature.

Dannheim, H., Riedel, T., Neumann-Schaal, M., Bunk, B., Schober, I., Spröer, C., *et al*. (2017) Manual curation and reannotation of the genomes of *Clostridium difficile* 630Δ*erm* and *C. difficile* 630. *J Med Microbiol* **66**: 286–293.

Day-Walsh, P., Shehata, E., Saha, S., Savva, G.M., Nemeckova, B., Speranza, J., *et al*. (2021) The use of an in-vitro batch fermentation (human colon) model for investigating mechanisms of TMA production from choline, L-carnitine and related precursors by the human gut microbiota. *Eur J Nutr* **60**: 3987–3999.

Du, Y., Shi, W.W., He, Y.X., Yang, Y.H., Zhou, C.Z., and Chen, Y. (2011) Structures of the substrate-binding protein provide insights into the multiple compatible solute binding specificities of the *Bacillus subtilis* ABC transporter OpuC. *Biochem J* **436**: 283–289.

Fichman, Y., Gerdes, S.Y., Kovács, H., Szabados, L., Zilberstein, A., and Csonka, L.N. (2015) Evolution of proline biosynthesis: enzymology, bioinformatics, genetics, and transcriptional regulation. *Biol Rev Camb Philos Soc* **90**: 1065–1099.

Fordtran, J.S., and Locklear, T.W. (1966) Ionic constituents and osmolality of gastric and small-intestinal fluids after eating. *Am J Dig Dis* **11**: 503–521.

Galinski, E.A., and Trüper, H.G. (1994) Microbial behaviour in salt-stressed ecosystems. *FEMS Microbiol Rev* **15**: 95–108.

Gregory, G.J., and Boyd, E.F. (2021) Stressed out: bacterial response to high salinity using compatible solute biosynthesis and uptake systems, lessons from Vibrionaceae. *Comput Struct Biotechnol J* **19**: 1014–1027.

Guarner, F., and Malagelada, J.R. (2003) Gut flora in health and disease. *Lancet* **361**: 512–519.

Guery, B., Galperine, T., and Barbut, F. (2019) *Clostridioides difficile*: diagnosis and treatments. *BMJ* **366**: l4609.

Gunde-Cimerman, N., Plemenitaš, A., and Oren, A. (2018) Strategies of adaptation of microorganisms of the three domains of life to high salt concentrations. *FEMS Microbiol Rev* **42**: 353–375.

Hall, I.C., and O'Toole, E. (1935) Intestinal flora in new-born infants: with a description of a new pathogenic anaerobe, *Bacillus difficilis*. *Am J Dis Child* **49**: 390–402.

Halmos, E.P., Christophersen, C.T., Bird, A.R., Shepherd, S. J., Gibson, P.R., and Muir, J.G. (2015) Diets that differ in their FODMAP content alter the colonic luminal microenvironment. *Gut* **64**: 93–100.

Harwood, C., and Archibald, A. (1990) Growth, maintenance and general techniques. In *Molecular Biological Methods for Bacillus*, Harwood, C.R., and Cutting, S.M. (eds). Chichester, New York: Wiley.

Heap, J.T., Kuehne, S.A., Ehsaan, M., Cartman, S.T., Cooksley, C.M., Scott, J.C., and Minton, N.P. (2010) The ClosTron: mutagenesis in *Clostridium* refined and streamlined. *J Microbiol Methods* **80**: 49–55.

Heap, J.T., Pennington, O.J., Cartman, S.T., Carter, G.P., and Minton, N.P. (2007) The ClosTron: a universal gene knock-out system for the genus *Clostridium*. *J Microbiol Methods* **70**: 452–464.

Herrou, J., Willett, J.W., Czyz, D.M., Babnigg, G., Kim, Y., and Crosson, S. (2017) Conserved ABC transport system regulated by the general stress response pathways of alpha- and gammaproteobacteria. *J Bacteriol* **199**: e00746-16.

Hoffmann, T., and Bremer, E. (2016) Management of osmotic stress by *Bacillus subtilis*: genetics and physiology. In *Stress and Environmental Regulation of Gene Expression and Adaptation in Bacteria*, de Bruijn, F.J. (ed). Hoboken, NJ, USA: John Wiley & Sons, pp. 657–676.

Hoffmann, T., and Bremer, E. (2017) Guardians in a stressful world: the Opu family of compatible solute transporters from *Bacillus subtilis*. *Biol Chem* **398**: 193–214.

Hoffmann, T., von Blohn, C., Stanek, A., Moses, S., Barzantny, H., and Bremer, E. (2012) Synthesis, release, and recapture of compatible solute proline by osmotically stressed *Bacillus subtilis* cells. *Appl Environ Microbiol* **78**: 5753–5762.

Hofmann, J.D., Biedendieck, R., Michel, A.-M., Schomburg, D., Jahn, D., and Neumann-Schaal, M. (2021) Influence of L-lactate and low glucose concentrations on the metabolism and the toxin formation of *Clostridioides difficile*. *PLoS One* **16**: e0244988.

Hofmann, J.D., Otto, A., Berges, M., Biedendieck, R., Michel, A.-M., Becher, D., *et al*. (2018) Metabolic reprogramming of *Clostridioides difficile* during the stationary phase with the induction of toxin production. *Front Microbiol* **9**: 1970.

Hopkins, R.J., and Wilson, R.B. (2018) Treatment of recurrent *Clostridium difficile* colitis: a narrative review. *Gastroenterol Rep* **6**: 21–28.

Horn, C., Sohn-Bösser, L., Breed, J., Welte, W., Schmitt, L., and Bremer, E. (2006) Molecular determinants for substrate specificity of the ligand-binding protein OpuAC from *Bacillus subtilis* for the compatible solutes glycine betaine and proline betaine. *J Mol Biol* **357**: 592–606.

Hussain, H.A., Roberts, A.P., and Mullany, P. (2005) Generation of an erythromycin-sensitive derivative of *Clostridium difficile* strain 630 (630Δ*erm*) and demonstration that the conjugative transposon Tn*916*ΔE enters the genome of this strain at multiple sites. *J Med Microbiol* **54**: 137–141.

Jenior, M.L., Leslie, J.L., Young, V.B., and Schloss, P.D. (2017) *Clostridium difficile* colonizes alternative nutrient niches during Infection across distinct murine gut microbiomes. *mSystems* **2**: e00063-17.

Kappes, R.M., Kempf, B., Kneip, S., Boch, J., Gade, J., Meier-Wagner, J., and Bremer, E. (1999) Two evolutionarily closely related ABC transporters mediate the uptake of choline for synthesis of the osmoprotectant glycine betaine in *Bacillus subtilis*. *Mol Microbiol* **32**: 203–216.

Kempf, B., and Bremer, E. (1998) Uptake and synthesis of compatible solutes as microbial stress responses to high-osmolality environments. *Arch Microbiol* **170**: 319–330.

Kim, L., Mogk, A., and Schumann, W. (1996) A xylose-inducible *Bacillus subtilis* integration vector and its application. *Gene* **181**: 71–76.

Koeth, R.A., Levison, B.S., Culley, M.K., Buffa, J.A., Wang, Z., Gregory, J.C., *et al*. (2014) γ-Butyrobetaine is a proatherogenic intermediate in gut microbial metabolism of L-carnitine to TMAO. *Cell Metab* **20**: 799–812.

Lessa, F.C., Mu, Y., Bamberg, W.M., Beldavs, Z.G., Dumyati, G.K., Dunn, J.R., *et al*. (2015) Burden of *Clostridium difficile* infection in the United States. *N Engl J Med* **372**: 825–834.

Neumann-Schaal, M., Hofmann, J.D., Will, S.E., and Schomburg, D. (2015) Time-resolved amino acid uptake of *Clostridium difficile* 630Δerm and concomitant fermentation product and toxin formation. *BMC Microbiol* **15**: 281.

Oswald, C., Smits, S.H.J., Höing, M., Sohn-Bösser, L., Dupont, L., Le Rudulier, D., *et al*. (2008) Crystal structures of the choline/acetylcholine substrate-binding protein ChoX from *Sinorhizobium meliloti* in the Liganded and Unliganded-closed states. *J Biol Chem* **283**: 32848–32859.

Overduin, J., Tylee, T.S., Frayo, R.S., and Cummings, D.E. (2014) Hyperosmolarity in the small intestine contributes to postprandial ghrelin suppression. *Am J Physiol Gastrointest Liver Physiol* **306**: G1108–G1116.

Perutka, J., Wang, W., Goerlitz, D., and Lambowitz, A.M. (2004) Use of computer-designed group II introns to disrupt *Escherichia coli* DExH/D-box protein and DNA helicase genes. *J Mol Biol* **336**: 421–439.

Pittelkow, M., Tschapek, B., Smits, S.H.J., Schmitt, L., and Bremer, E. (2011) The crystal structure of the substrate-binding protein OpuBC from *Bacillus subtilis* in complex with choline. *J Mol Biol* **411**: 53–67.

Purdy, D., O'Keeffe, T.A.T., Elmore, M., Herbert, M., McLeod, A., Bokori-Brown, M., *et al*. (2002) Conjugative transfer of clostridial shuttle vectors from *Escherichia coli* to *Clostridium difficile* through circumvention of the restriction barrier. *Mol Microbiol* **46**: 439–452.

Robayo-Torres, C.C., Quezada-Calvillo, R., and Nichols, B.L. (2006) Disaccharide digestion: clinical and molecular aspects. *Clin Gastroenterol Hepatol* **4**: 276–287.

Robinson, J.I., Weir, W.H., Crowley, J.R., Hink, T., Reske, K. A., Kwon, J.H., *et al*. (2019) Metabolomic networks connect host-microbiome processes to human *Clostridioides difficile* infections. *J Clin Invest* **129**: 3792–3806.

Ruiz, S.J., Schuurman-Wolters, G.K., and Poolman, B. (2016) Crystal structure of the substrate-binding domain from *Listeria monocytogenes* bile-resistance determinant BilE. *Crystals* **6**: 162.

Rupnik, M., Wilcox, M.H., and Gerding, D.N. (2009) *Clostridium difficile* infection: new developments in epidemiology and pathogenesis. *Nat Rev Microbiol* **7**: 526–536.

Schäffler, H., and Breitrück, A. (2018) *Clostridium difficile* – from colonization to infection. *Front Microbiol* **9**: 646.

Schiefner, A., Breed, J., Bösser, L., Kneip, S., Gade, J., Holtmann, G., *et al*. (2004) Cation-π interactions as determinants for binding of the compatible solutes glycine betaine and proline betaine by the periplasmic ligand-binding protein ProX from *Escherichia coli*. *J Biol Chem* **279**: 5588–5596.

Shah, D.N., Aitken, S.L., Barragan, L.F., Bozorgui, S., Goddu, S., Navarro, M.E., *et al*. (2016) Economic burden of primary compared with recurrent *Clostridium difficile* infection in hospitalized patients: a prospective cohort study. *J Hosp Infect* **93**: 286–289.

Sikkema, H.R., Van Den Noort, M., Rheinberger, J., De Boer, M., Krepel, S.T., Schuurman-Wolters, G.K., *et al*. (2020) Gating by ionic strength and safety check by cyclic-di-AMP in the ABC transporter OpuA. *Sci Adv* **6**: eabd7697.

Simó, C., and García-Cañas, V. (2020) Dietary bioactive ingredients to modulate the gut microbiota-derived metabolite TMAO. New opportunities for functional food development. *Food Funct* **11**: 6745–6776.

Sleator, R.D., Clifford, T., and Hill, C. (2007) Gut osmolarity: a key environmental cue initiating the gastrointestinal

phase of *Listeria monocytogenes* infection? *Med Hypotheses* **69**: 1090–1092.
Sleator, R.D., and Hill, C. (2001) Bacterial osmoadaptation: the role of osmolytes in bacterial stress and virulence. *FEMS Microbiol Rev* **26**: 49–71.
Teichmann, L., Chen, C., Hoffmann, T., Smits, S.H.J., Schmitt, L., and Bremer, E. (2017) From substrate specificity to promiscuity: hybrid ABC transporters for osmoprotectants. *Mol Microbiol* **104**: 761–780.
Teichmann, L., Kümmel, H., Warmbold, B., and Bremer, E. (2018) OpuF, a new *Bacillus* compatible solute ABC transporter with a substrate-binding protein fused to the transmembrane domain. *Appl Environ Microbiol* **84**: e01728-18.
Theriot, C.M., Koenigsknecht, M.J., Carlson, P.E., Hatton, G. E., Nelson, A.M., Li, B., *et al*. (2014) Antibiotic-induced shifts in the mouse gut microbiome and metabolome increase susceptibility to *Clostridium difficile* infection. *Nat Commun* **5**: 3114.
van den Berg, J., Boersma, A.J., and Poolman, B. (2017) Microorganisms maintain crowding homeostasis. *Nat Rev Microbiol* **15**: 309–318.
Vijaranakul, U., Nadakavukaren, M.J., Bayles, D.O., Wilkinson, B.J., and Jayaswal, R.K. (1997) Characterization of an NaCl-sensitive *Staphylococcus aureus* mutant and rescue of the NaCl-sensitive phenotype by glycine betaine but not by other compatible solutes. *Appl Environ Microbiol* **63**: 1889–1897.
Vijaranakul, U., Nadakavukaren, M.J., De Jonge, B.L.M., Wilkinson, B.J., and Jayaswal, R.K. (1995) Increased cell size and shortened peptidoglycan interpeptide bridge of NaCl-stressed *Staphylococcus aureus* and their reversal by glycine betaine. *J Bacteriol* **177**: 5116–5121.
Waterhouse, A., Bertoni, M., Bienert, S., Studer, G., Tauriello, G., Gumienny, R., *et al*. (2018) SWISS-MODEL: homology modelling of protein structures and complexes. *Nucleic Acids Res* **46**: W296–W303.
Will, S.E., Henke, P., Boedeker, C., Huang, S., Brinkmann, H., Rohde, M., *et al*. (2019) Day and night: metabolic profiles and evolutionary relationships of six axenic non-marine cyanobacteria. *Genome Biol Evol* **11**: 270–294.
Wolf, J., Stark, H., Fafenrot, K., Albersmeier, A., Pham, T.K., Müller, K.B., *et al*. (2016) A systems biology approach reveals major metabolic changes in the thermoacidophilic archaeon *Sulfolobus solfataricus* in response to the carbon source L-fucose versus D-glucose. *Mol Microbiol* **102**: 882–908.
Wood, J.M. (2011) Bacterial osmoregulation: a paradigm for the study of cellular homeostasis. *Annu Rev Microbiol* **65**: 215–238.
Wood, J.M., Bremer, E., Csonka, L.N., Kraemer, R., Poolman, B., van der Heide, T., and Smith, L.T. (2001) Osmosensing and osmoregulatory compatible solute accumulation by bacteria. *Comp Biochem Physiol - A Mol Integr Physiol* **130**: 437–460.
Zhang, D., Prabhu, V.S., and Marcella, S.W. (2018) Attributable healthcare resource utilization and costs for patients with primary and recurrent *Clostridium difficile* infection in the United States. *Clin Infect Dis* **66**: 1326–1332.

Supporting Information

Additional Supporting Information may be found in the online version of this article at the publisher's web-site:

Fig. S1. Osmolarity of the employed growth media.

Fig. S2. Plasmid constructs designed for the heterologous expression of *C*. *difficile* transporter genes in *B*. *subtilis* TMB118. Shown are the constructs consisting of the P_{opuC} of *B*. *subtilis* fused to the respective transporter encoded by **(A)** CDIF620erm_01020/01021 or **(B)** CDIF620erm_03509/03510. Highlighted are the −35 and − 10 boxes and the ribosomal binding sites (RBS). Both constructs were flanked by the recognition site for the restriction enzyme *XbaI* for cloning into the plasmid pX that was used for stable integration into the genome of *B*. *subtilis* TMB118.

Fig. S3. Growth of *B*. *subtilis* JH642, TMB118, AM01 and AM02 with different compatible solutes. Shown are the growth curves of *B*. *subtilis* **(A)** JH642, **(B)** TMB118, **(C)** AM01 stably expressing the transporter encoded by CDIF620erm_01020/01021 and **(D)** AM02 stably expressing the transporter encoded by CDIF620erm_03509/03510 in SMM or in SMM containing 1 M NaCl or SMM containing 1 M NaCl and 1 mM of carnitine, glycine betaine, γ-butyrobetaine, crotonobetaine, choline, homobetaine, proline betaine, DMSP, ectoine, and proline. Measurements of scattered light intensities (SLI) at 620 nm over 26 h are shown. Growth experiments were performed with at least four biological and three technical replicates. The standard deviation is given.

Table S1. Composition of the defined MDM growth medium for *C*. *difficile*

Table S2. Comparative exo-metabolome analysis of *C*. *difficile* wild type and Δ*opuFB* mutant at high osmolarity conditions with or without carnitine in comparison to unstressed conditions. Experiments were performed with at least four biological and three technical replicates.

Table S3. Comparative metabolome and exo-metabolome analysis of *C*. *difficile* wild type grown under high osmolarity conditions with or without carnitine in comparison to unstressed conditions. Tabs 'Intracellular_Overview' and 'Intracellular_FC' summarize the wild type intracellular fermentation profile grown under high osmolarity conditions with or without carnitine in comparison to unstressed conditions (short-term). Tabs 'Extracellular_Overview' and 'Extracellular_FC' list the extracellular fermentation profile grown under high osmolarity conditions with or without carnitine in comparison to unstressed conditions (short-term). Tabs 'extracellular_aa_overview' and 'extracellular_aa_FC' enumerate the extracellular amino acid abundances of the wild type strain grown under high osmolarity conditions with or without carnitine in comparison to unstressed conditions (short-term). Tabs 'non-volatile major metabolites' and 'volatile fermentation products' summarize the abundant intracellular metabolites and the fermentation profile during long-term adaptation of the wild-type. Experiments rely on five independent replicates (major experiment) or four independent replicates (long-term adaptation).